Molecular engineering of triphenylamine -based metal-free organic dyes for dye-sensitized solar cells

Faezeh Pakravesh, Mohammad Izadyar*, and Foroogh Arkan

Computational Chemistry Research Laboratory, Department of Chemistry, Faculty of Science, Ferdowsi University of Mashhad, Mashhad, Iran

* Corresponding author.

E-mail address: izadyar@um.ac.ir

Abstract

In this study, the photovoltaic properties of the organic dyes based on triphenylamine having a D-π-A structure including TC201, TC202, TC203, TC601, H-P, F-P, FF-P, T-F, and P1B were investigated theoretically. In this model, triphenylamine was used as an electron donor, cyanoacrylic acid, and benzoic acid as the electron acceptors, and anthracene phenyl, anthracene vinyl phenyl, anthracene ethynyl phenyl, ethynyl anthracene phenyl, styryl phenyl, styryl-2-fluorophenyl, styryl-2,6-difluorophenyl, styryl furan, and styryl as the π-conjugated systems. The results show that a change in the π-conjugated system and electron acceptor affect the properties of the dye-sensitized solar cell (DSSC). Also, TC601 dye having the ethynyl anthracene phenyl π-conjugated system shows

the highest charge transfer distance (D_{CT}) and the least overlap of the electron-hole distribution (S) in comparison with other dyes. Moreover, the presence of a triple bond in the vicinity of triphenylamine increases the resonance effect of the π-electrons that facilitates the process of charge transfer in this dye. Spectroscopic analysis shows that H-P and F-P dyes have the higher molecular absorption coefficients and TC202, TC203, F-P, and T-F dyes show a red shift in comparison with other dyes. Moreover, the voltage-current curve of the studied dyes shows that the highest values of the open circuit voltage and short circuit current density are related to P1B and TC601 dyes, respectively. Finally, TC601 and P1B are proposed as the best candidates to be used in the DSSCs due to their maximum incident photon to current conversion efficiency.

1 │ INTRODUCTION

The common essential sources of energy production are fossil fuels such as coal, oil and natural gas, which make up about 80% of total energy consumption.[1-3] But these resources are not unlimited and will be completed in the near future. On the other hand, energy demand has increased due to population growth and urbanization.[4] Also, the global economy is remarkably related to energy because it includes all aspects of life and human activities.[5] Therefore, to deal with such a

massive demand for energy, we must use renewable sources, such as hydropower, wind energy, solar energy, geothermal energy, and biomass energy, in which solar energy is abundant, cheap, available, no polluting and unique natural source of clean energy.[6-10] New technology for using solar energy is the solar cell, that converts solar light directly into electricity without any environmental pollution. [11,12] Dye-sensitized solar cells (DSSCs) as the third generation of the solar cells, developed by O'Regan and Grätzel,[13] have received a lot of attention due to advantages, such as simple manufacturing process, low cost, environmental compatibility, flexibility, transparency, and having a variety of dyes.[14-18] A typical DSSC consists of a transparent conducting oxide (TCO), dye sensitizer, mesoporous TiO_2 film, the counter electrode (Pt), and electrolyte (I^-/I^-_3).[19-21]

According to the working principles of the DSSC, when sunlight collides the surface of the solar cell, the photon is absorbed by the dye. Then the electron is transferred from the highest occupied molecular orbital (HOMO) to the lowest unoccupied molecular orbital (LUMO) level, and electron-driving force transfers the electron to the TiO_2 conduction band (CB). Then, electron flows to the external circuit and the cathode, generating electricity. Finally, the oxidized dye supplies the lost electron through the electrolyte.[22-24]

One of the high-performance dyes in the DSSC is ruthenium-based dyes, in which the best-known compounds are N3, N719, and N749.[25] These dyes have a

strong absorption band in the visible area. The presence of various ligands in their structure increases the efficiency of the solar cells.[26] The main problem in using these dyes is the presence of toxic metals, which is a danger for the environment. [27] Also, due to the high cost of these dyes, other dyes, such as metal-free organic dyes, including coumarin,[28] triphenylamine,[29] indoline,[30] and porphyrin,[31] which have advantages such as low synthesis cost, high molar absorption coefficient, simple synthesis, tunable optical properties and environmental compatibility.[32-36]

There are various types of structures for organic dyes, including D-π-A,[37] D-D-π-A,[38] D-A-π-A,[39] and D-π_1-π_2-A,[40] where D is the electron donor, π is the conjugated bridge and A is the electron acceptor. D-π-A architecture improves the π-conjugation effect and impressive electron injection to the semiconductor surface.[41] There are some samples of metal-free organic dyes designed to improve the efficiency of the solar cells. For example, in 2015, two metal-free organic dyes based on thioindigo having a D-π-A structure called D1 and D2 within acrylic acid and cyanoacrylic acid as electron acceptors were designed.[42] The obtained results reveal that D2 dye with cyanoacrylic acid electron acceptor has the high values of open-circuit voltage, short-circuit current density, fill factor, and efficiency than D1. This behavior can be explained by the advanced electron-withdrawing ability of the cyanoacrylic acid than acrylic acid.

Li et al compared the photovoltaic properties of three metal-free organic dyes containing pyrrolo[3,2,1-kl]- phenothiazine moiety as the electron donor, different π-bridges including thiophene (JY40), furan (JY41) and terthiophene (JY42) and cyanoacrylic acid as the electron acceptor.[43] The obtained results indicate that JY42 dye having terthiophene as the π-bridge shows the highest efficiency of 7.54% and short-circuit current density of 17.76 mA/cm^{-2}. Also, the dye absorption spectrum shows that JY42 dye having terthiophene π-bridge represents the highest amount of molar absorption coefficient and red-shift in comparison with other dyes.

A series of metal-free dyes based on the reference dye of IC-2 for evaluating the effect of the π-bridges was designed.[44] The results show that S7 dye having the 5-(thiazol-5yl)thiazole π-bridge exhibits the lowest value of the energy gap due to greater electron deficiency. Also, the absorption spectra of all studied dyes show a greater red-shift than that of the reference dye (IC-2), in which S7 dye has the highest maximum wavelength due to higher oscillating strength.

Naik et al investigated the photovoltaic properties of P1, P2, P3, and P4 dyes with a D-π-A structure and different electron acceptors, such as cyanoacetic acid, rhodanine-3-acetic acid, barbituric acid, and thiobarbituric acid.[45] The LUMO levels of these dyes are higher than that of TiO$_2$, confirming that electrons in the excited state can be transferred to the TiO$_2$ semiconductor. Also, the HOMO levels

of these dyes are lower than the redox potential of the electrolyte, which indicates that there is enough energy to reproduce the dye. Based on the results, P1 has a great incident photon to current conversion efficiency (IPCE) than other dyes.

As mentioned above, triphenylamine is one of the metal-free organic dyes with strong electron-donating ability due to the π-bonds of the aromatic rings, as well as the presence of a lone pair electron on the nitrogen atom.[46,47] Due to the non-planar structure, this dye does not aggregate on the semiconductor surface, showing good electron-hole transfer properties.[48-50] Triphenylamine has a good π-conjugated system that improves the photovoltaic properties, such as light-harvesting efficiency (LHE), short-circuit current density (J_{SC}), and incident photon to current conversion efficiency (IPCE).[51] Considering all the mentioned properties of the triphenylamine-based dyes, they are widely used in the DSSCs.

In 2018, three organic dyes based on triphenylamine with mono-, di-, and tri-cyanoacrylic acid as an anchor group and thiophene as the π-bridges were analyzed by Wazzan et al.[52] The study of the frontier molecular orbitals, absorption spectrum, light-harvesting efficiency and Gibbs energy change of the dye regeneration showed that the dyes having a lot of anchor groups exhibit proper optical and electronic properties. Also, TPA3T2A and TPA3T2A dyes show an acceptable intra-molecular charge transfer, longer charge transfer distance, and greater dipole moment. Moreover, in 2019, triphenylamine-based dyes were

investigated to realize the effect of electron donors on the photovoltaic properties of the DSSCs. The results show that an increase in the number of electron donor groups improves the LHE, open-circuit voltage (V_{OC}), short-circuit current density (J_{SC}) and Gibbs energy change of the electron injection (ΔG_{inj}).[53]

Herein, we theoretically investigate the photovoltaic properties of some organic dyes based on triphenylamine having a D-π-A structure including TC201, TC202, TC203, TC601, H-P, F-P, FF-P, T-F, and P1B dynamically and kinetically. [54-57] Triphenylamine was used as an electron donor, cyanoacrylic acid and benzoic acid as an electron acceptor and anthracene phenyl, anthracene vinyl phenyl, anthracene ethynyl phenyl, ethynyl anthracene phenyl, styryl phenyl, styryl-2-fluorophenyl, styryl-2,6-difluorophenyl, styryl furan, and styryl as the π-conjugated system. Moreover, to have a better understanding of the designed solar cells, the dye absorption spectra were simulated. LHE and IPCE as the functions of the absorption wavelength, within the kinetics parameters of the excitation processes and voltage-current behavior, were analyzed.

2 │ COMPUTATIONAL DETAILS

Density functional theory (DFT) and time dependent-density functional theory (TD-DFT) was used for calculation ground and excited states of triphenylamine-based dyes, respectively.[58,59] Also, NBO analysis was used to describe and achieve the energy values of the frontier molecular orbitals at the

M06-2X/6-311++G(2d,2p) level of theory.[60] Moreover, the Multiwfn program was used to obtain the overlap indices and electron-hole separation in the DSSCs.[61] All calculations were carried out by using Gaussian 09 package.[62]

The DSSC efficiency was calculated based on the open-circuit voltage, short-circuit current density and fill factor (Equation (1)).[63]

$$\eta_0 = \frac{J_{SC} . V_{OC} . FF}{P_\text{in}} \qquad (1)$$

where P_in is the input power of the solar cell. Open-circuit voltage is defined as the voltage generated in the radiating photovoltaic device when no external charge is connected that is expressed by Equation (2):[64]

$$V_{OC} = \frac{K . T_{cell}}{q} \ln \frac{J_{SC}}{J_0} \qquad (2)$$

where K_B is the Boltzmann constant, T_{cell} is the temperature of the solar cell, q is the unit charge and J_0 is the saturation current density evaluated by Equation (3):[65]

$$J_0 = 2.95 \times 10^5 \exp \left(\frac{-E_g}{K_B T_{cell}} \right) \qquad (3)$$

Short-circuit current density means current flowing through the photovoltaic device when the device is irradiated and the electrodes are connected. J_{SC} is calculated according to Equation (4):[66]

$$J_{SC} = \int_1^2 q . IPCE() () d \qquad (4)$$

where $\Phi(\lambda)$ is the incident photon flux at a given wavelength, and IPCE is an incident photon-to-current conversion efficiency, which can be described by Equation (5):[67]

$$IPCE = LHE\ (\lambda).\Phi_{inj}.\eta_{coll} \qquad (5)$$

where Φ_{inj} is the electron injection efficiency, η_{coll} is the charge collection efficiency and LHE is the light-harvesting efficiency that can be estimated by Equation (6):[68]

$$LHE = 1\text{-}10^{-f} \qquad (6)$$

where f is the oscillating strength that is determined from the TD-DFT analysis, directly. Fill factor is a parameter that exhibits the general behavior of a solar cell, obtained from Equation (7):[69]

$$FF = \frac{oc - \ln(oc - 0.72)}{(oc + 1)}(7)$$

where ϑ_{oc} is defined as the normalized V_{OC} calculated by Equation (8):[69]

$$\vartheta oc = \frac{qV_{OC}}{K_B T}(8)$$

The Gibbs energy of the electron injection from the excited states of the dye to the semiconductor conduction band, (ΔG_{ing}), is evaluated according to Equation (9):[70]

$$\Delta G_{inj} = E_{OX(dye)*} - E_{CB} \qquad (9)$$

where $E_{OX(dye)*}$ is the oxidation potential of dye in the excited state and E_{CB} is the energy of the semiconductor conduction band (TiO$_2$). The Gibbs energy of the dye regeneration can be expressed by Equation (10):[71]

$$\Delta G_{reg} = E_{OX(dye)} - E_{redox(electrolyte)} \qquad (10)$$

where $E_{OX(dye)}$ and E_{redox} are the oxidation potential of the dye in the ground state and redox potential of the electrolyte, respectively. Moreover, another important parameter that can be obtained theoretically is the exciton binding energy, EBE, which is evaluated by Equation (11):[72]

$$EBE = E_{gap.elec} - E_{0-0} \qquad (11)$$

where E_{0-0} is the vertical excitation energy and E_{gap} is the band gap energy of the dye. In addition to examining the parameters related to the dynamics of charge transfer in the solar cell, a kinetics study of the solar cell processes is important. The rate constant of the electron injection in the dye/TiO$_2$ interface (k_{inj}) is calculated by Equation (12):[73]

$$k_{inj} = \frac{\square^{0.5}}{\hbar(E_{0-0}K_BT)^{0.5}} |V_{RP}|^2 \exp[-¿¿¿] \qquad (12)$$

where $\hbar$ is the reduced Planck constant, and V_{RP} is the coupling constant between the dye and TiO$_2$ surface determined by Equation (13):[74]

$$|V_{RP}| = \frac{E_{HOMO} - E_{CB,TiO2}}{2} \qquad (13)$$

Upon illumination, the electrons in the dye molecules are excited from the HOMO to the LUMO levels, creating a hole in the HOMO level. Thus, an electron-hole pair, exciton, is formed by a strong Coulomb interaction between this pair. The material-dependent constant, α, showing the ratio of the Coulomb and exchange interactions between the electron and hole can be described by Equation (14):[75]

$$EBE = \frac{(-1)^2 \square_x e^4 k^2}{2\square^2 \hbar^2 \square^2} \tag{14}$$

where ε is the dielectric constant of the donor component, $\hbar$ is the reduced Planck's constant, ε_o is the vacuum permittivity, μ_x is the reduced mass of the exciton, e is the electronic charge and $k = (4\pi\varepsilon_o)^{-1} = 9 \times 10^9$ N m^2 C^{-2}.

The rate of photon absorption, R_a^s, is evaluated according to Equation (15):[76]

$$R_a^S = \frac{4\,k\,e^2 \left(E_{LUMO} - E_{HOMO}\right)^3 a_x^{\,2}}{3\,c^3\,\square^{1.5}\,\hbar^4} \tag{15}$$

In this equation, c is the speed of light and a_x is the radius of Bohr's exciton, which is expressed by Equation (16):[77]

$$a_x = \frac{\square^2}{(-1)^2{}_X}\,a_0 \tag{16}$$

where μ is the reduced mass of the electron in a hydrogen atom and a_0 is the Bohr radius. The exciton dissociation rate, R_d, can be obtained from Equation (17):[78]

$$R_d = \frac{8\square^2}{3\hbar^3\square^2 E_B} \left[E_{LUMO}^D - E_{CB}^A - E_B\right]^2 (\hbar\omega_\vartheta)\ \mu_x\ a_x^2 \qquad (17)$$

where ω_ϑ is the frequency of the incident phonon to the dyes.

Quantum reactivity indices include electronic chemical hardness (η_e), electronic chemical potential (μ), and global electrophilicity (ω). Chemical hardness is a useful parameter for understanding the chemical behavior of the dyes, which is assumed as the resistance to charge transfer obtained by Equation (18):[79]

$$\eta_e = E_{LUMO} - E_{HOMO} \qquad (18)$$

The electronic chemical potential indicates the tendency for electrons to escape into a molecular system, which is determined Equation (19):[80]

$$\mu = \frac{E_{HOMO} + E_{LUMO}}{2} \qquad (19)$$

The global electrophilicity index, ω, is calculated through Equation (20):[81]

$$\omega = \frac{\square^2}{2\square_e} \qquad (20)$$

To have an insight into the solar cell photovoltaic processes, the analysis of charge transfer characteristics is necessary. One important parameter for describing the charge transfer is D_{CT}, which is defined as the distance between two barycenters (r^+ and r^-) obtained from Equation (21):[82]

$$D_{CT} = \dot{\iota} \qquad (21)$$

Another charge transfer parameter is the overlap of the e-h distributions (S), which is determined by Equation (22):[83]

$$\sqrt{C_{-¿(r)/A_{-¿}}dr¿}\ ¿\ S_{\pm}=\int\ \sqrt{C_{+¿(r)/A_{+¿}}}\ ¿\ ¿ \tag{22}$$

where A is the normalization factor and C^+ (r) and C^- (r) are equal to ρ^+ (r) and ρ^- (r) integrals. Another charge transfer parameter is the scale of e-h separation (t), which is given by Equation (23):[84]

$$t=D_{CT}-H \tag{23}$$

where H represents the half of the sum of two centroid axis along the direction of electron transfer.

3 │ RESULTS AND DISCUSSION

3.1 │ Structural and electronic properties of the dyes

The structures of nine metal-free organic dyes with the D-π-A design consists of triphenylamine as an electron donor, cyanoacrylic acid and benzoic acid as the electron acceptors and different π-conjugated system were optimized at the M06-2X/6-311++G (2d,2p) level of theory. These compounds include TC201 ((E)-2 cyano-3-(4-(10-(4-(diphenylamino)phenyl)anthracene-9-yl)phenyl)acrylic acid), TC 202 ((E)-2-cyano-3-(4-((E)-2-(10-(4-(diphenylamino)phenyl)anthracene-9-yl)vinyl)phenyl)yl)vinyl)phenyl)acrylic acid), TC203 ((E)-2-cyano-3-(4-((10-(4-(diphenyla mino)phenyl)anthracene-9-yl)etynyl)phenyl)acrylic acid, TC601 ((E)-2-

cyano-3-(4-(10-((4-diphenylamino)phenyl)ethynyl)anthracene-9-yl)phenyl)acrylic

acid), H-P ((E)-3-(4-((E)-4-diphenylaminostyryl)phenyl)-2-cyanoacrylic acid), F-P

((E)-3-(4-((E)-4-diphenylaminostyryl)-2-fluorophenyl)-2-cyanoacrylic acid), FF-P

((E)-3-(4-((E)-4-diphenylaminostyryl)-2,6-difluorophenyl)-2-cyanoacrylic acid),

T-F ((E)-2-cyano-3-(5-(E-4-(diphenylamino)styryl)furan-2-yl)acrylic acid), P1B

((E)-p-(p'-(diphenylamino)styryl)benzoic acid). The optimized structures of these

dyes and their relative electronic energies are represented in Figure 1.
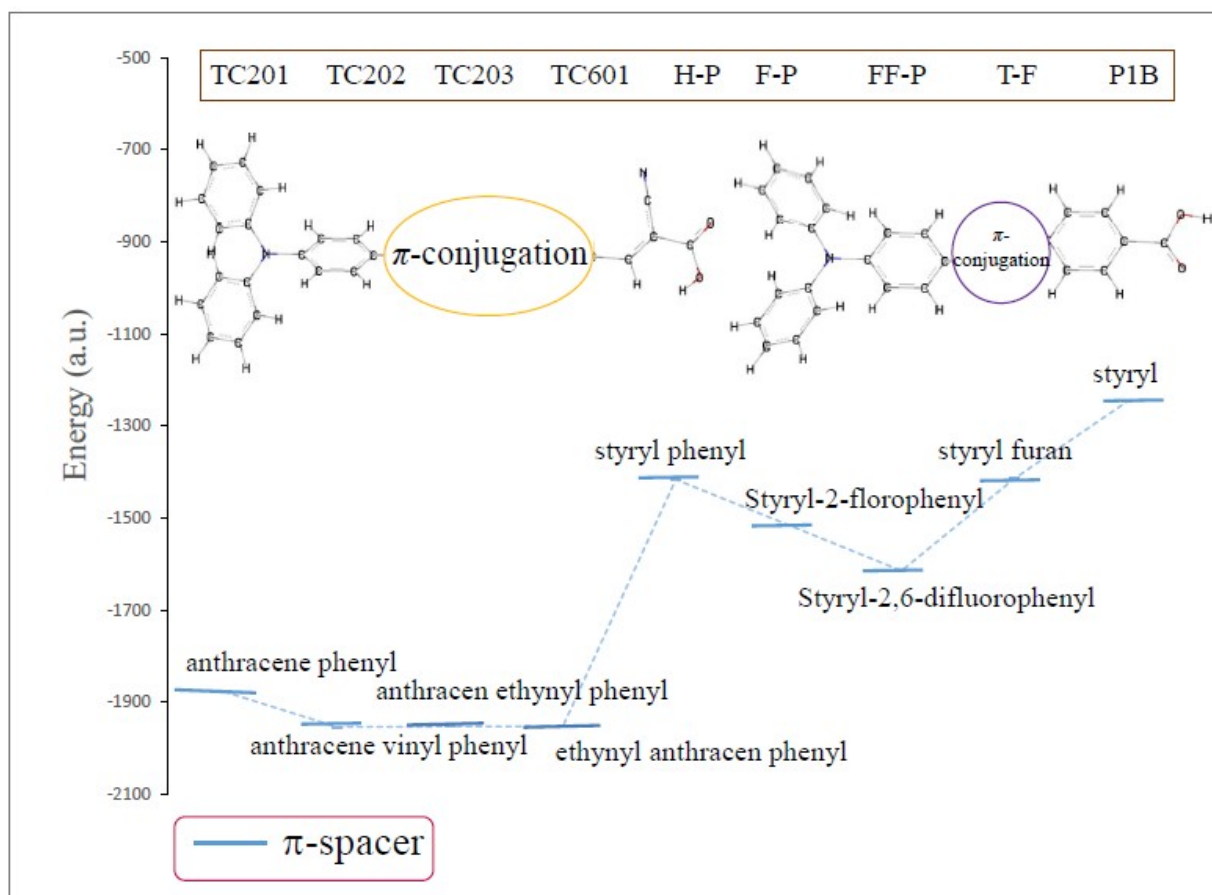
FIGURE 1 Optimized structures of the studied dyes within the electronic energies.

NBO analysis was used to investigate the energy levels of HOMO, HOMO-n and LUMO, LUMO+n, electron transfer from the dye to TiO_2, and dye regeneration. According to Figure 2, the energy level of LUMO in all these compounds is higher than the TiO_2 conduction band, which indicates that the electron transfer from the dye to the semiconductor is optimal. Also, their HOMO energy level is below the redox potential of the electrolyte (I^-/I^-_3), which indicates that dye regeneration is effective.
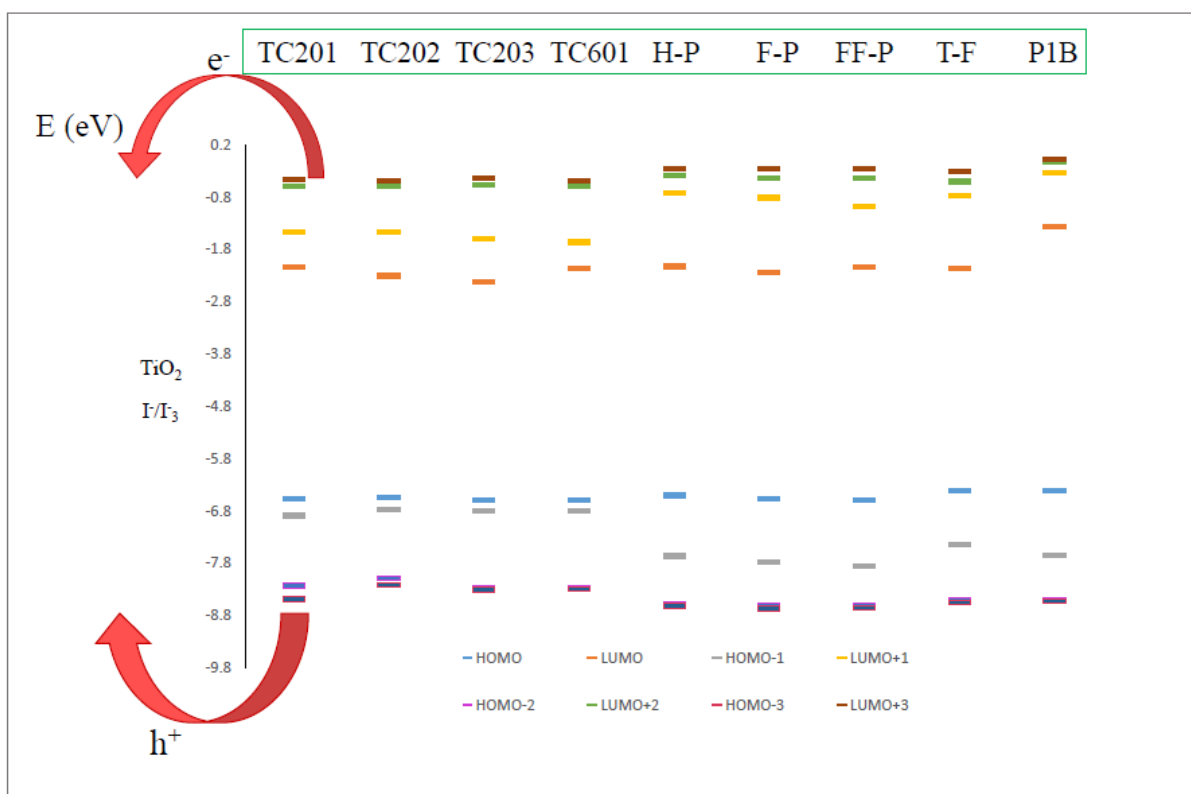
FIGURE 2 Energy diagram of the frontier molecular orbitals of the dyes, TiO_2 and electrolyte I^- / I^-_3.

The energies of the frontier molecular orbitals of the dyes, quantum reactivity indices including electron chemical hardness (η_e), electron chemical potential (μ) and global electrophilicity (ω), Gibbs energy of the electron injection from the dye to TiO_2 (ΔG_{inj}), Gibbs energy of dye regeneration (ΔG_{reg}) and electron-driving force (eV_{OC}) were calculated and shown in Table 1. According to Table 1, negative values of ΔG_{inj} indicate that the process of charge transfer from the dye in the excited state to TiO_2 occurs spontaneously. Among these compounds, TC601 has the least value of the Gibbs energy showing that the process of electron transfer occurs more properly. Moreover, the negative character of ΔG_{reg} makes the dye regeneration process favorable.

TABLE 1 HOMO and LUMO energy levels of the dyes, electronic chemical hardness (η_e), electronic chemical potential (μ), global electrophilicity (ω), Gibbs energy of the electron injection (ΔG_{inj}), Gibbs energy of the dye regeneration (ΔG_{reg}) and electron-driving force (eV_{OC}).

Dye	-HOMO (eV)	-LUMO (eV)	η_ϵ (eV)	$-\mu$ (eV)	ω (eV)	$-\Delta G_{inj}$ (eV)	$-\Delta G_{reg}$ (eV)	eV_{OC} (eV)
TC201	6.57	2.14	4.43	4.35	2.14	0.67	1.72	1.86
TC202	6.54	2.30	4.24	4.42	2.30	0.44	1.69	1.70
TC203	6.59	2.43	4.16	4.51	2.44	0.27	1.74	1.57
TC601	6.60	2.16	4.44	4.38	2.16	1.43	1.75	1.84

								
H-P	6.50	2.12	4.38	4.31	2.12	0.55	1.65	1.88
F-P	6.57	2.23	4.34	4.40	2.23	0.45	1.72	1.77
FF-P	6.59	2.14	4.45	4.36	2.14	0.52	1.74	1.86
T-F	6.41	2.16	4.25	4.28	2.16	0.39	1.56	1.84
P1B	6.41	1.37	5.04	3.89	1.50	1.01	1.56	2.63

Based on the data in Table 1, the values of the dyes electrophilicity, which indicate the degree of dye tendency to absorb electrons are in contrast with the eV_{OC} values. This means that a decrease in electrophilicity increases the electron-driving force to the semiconductor. The theoretical trends in ω and eV_{OC} of the dyes are respectively according to:

P1B < H-P < TC201 < FF-P < T-F < TC601 < F-P < TC202 < TC203

TC203 < TC202 < F-P < TC601< T-F < FF-P < TC201 < H-P < P1B,

The linear relationship between the eV_{OC} and the electronic chemical potential and electrophilicity characteristics of all dyes is shown in Figure 3. By reducing the absolute value of the electronic chemical potential, the eV_{OC} values of the dyes increase, which elevates the electron tendency for escaping from the molecular system and facilitates the electron transfer from the dye to the semiconductor. Also, the reduction of electrophilicity reduces the tendency of electron-accepting that increases the electron-driving force to the semiconductor.
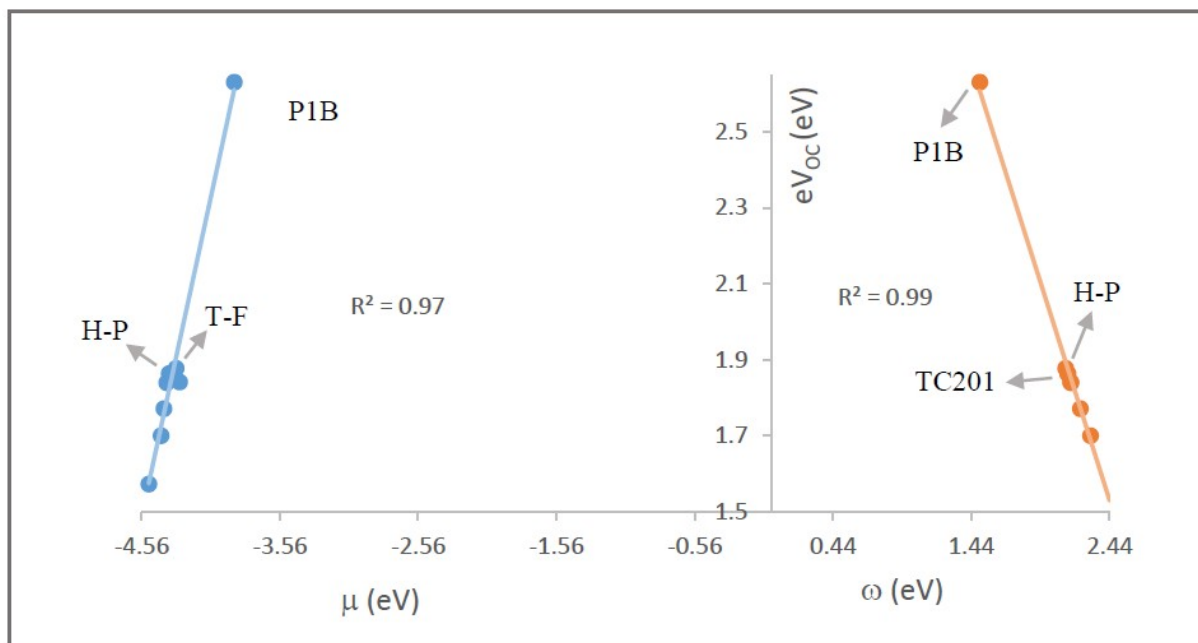
**FIGURE 3** Linear correlations of the eV_{OC} vs ω and μ.

Also, based on Figure 4, the dihedral angles between the electron acceptor group and the π-conjugated system in the TC201, TC202, TC203, TC601, HP, FP, and P1B dyes, as well as the electron-donor group and the π-conjugated system in the FF-P and T-F dyes approximately equal to 180°, which indicates that the A-π and D-π parts of these dyes are planers, making the charge transfer desirable.
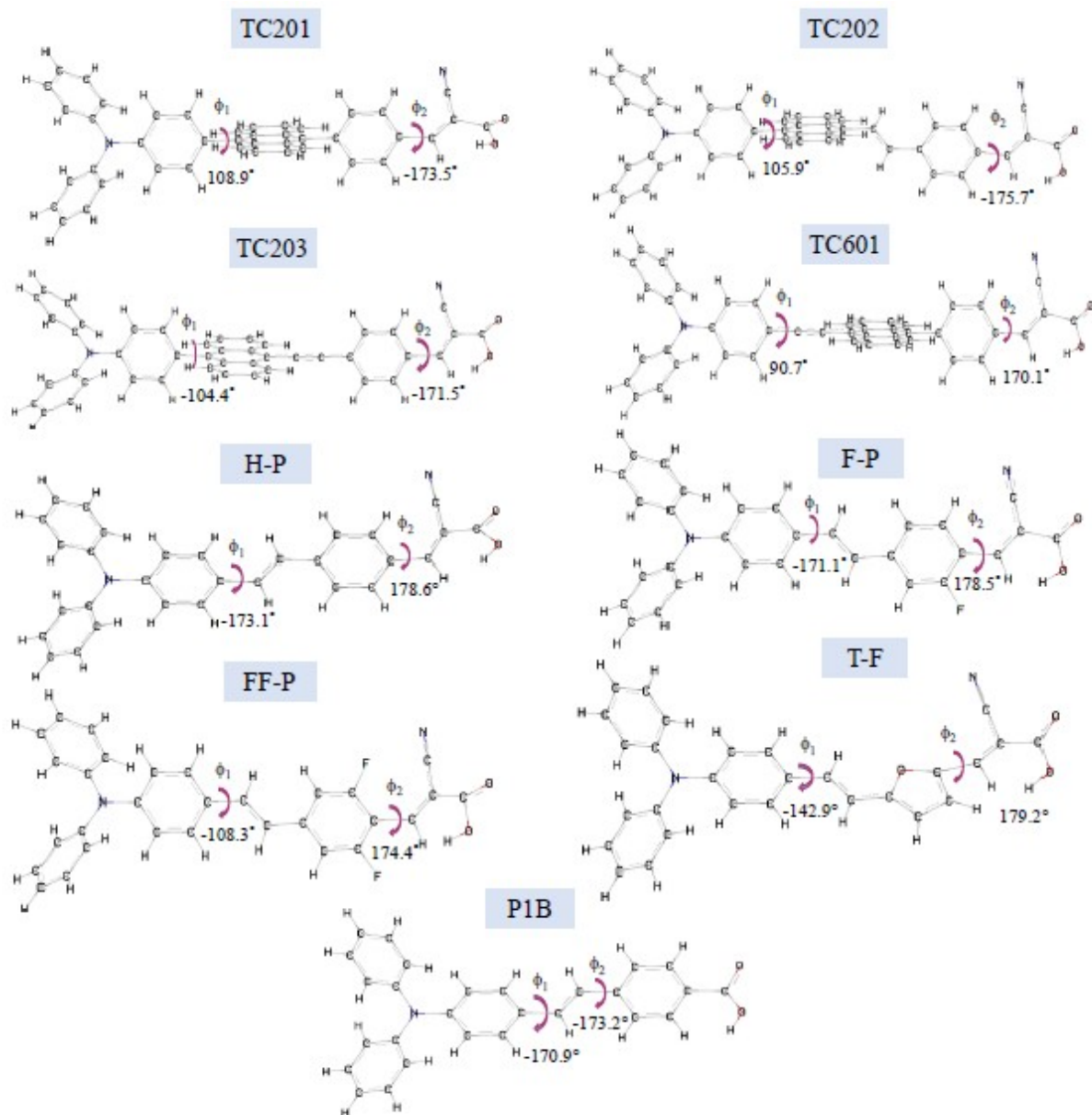
FIGURE 4 Dihedral angles between different parts of the dye structures.

The electron density distribution of the frontier molecular orbitals in the molecular structures of these dyes is shown in Figure 5. According to Figure 5, the electron density of HOMO is mainly distributed over the electron donor moieties, while LUMO is distributed over the electron acceptor parts. This property indicates

a good overlap between the molecular orbitals and increases the intra-molecular charge transfer from the electron donor to the acceptor.
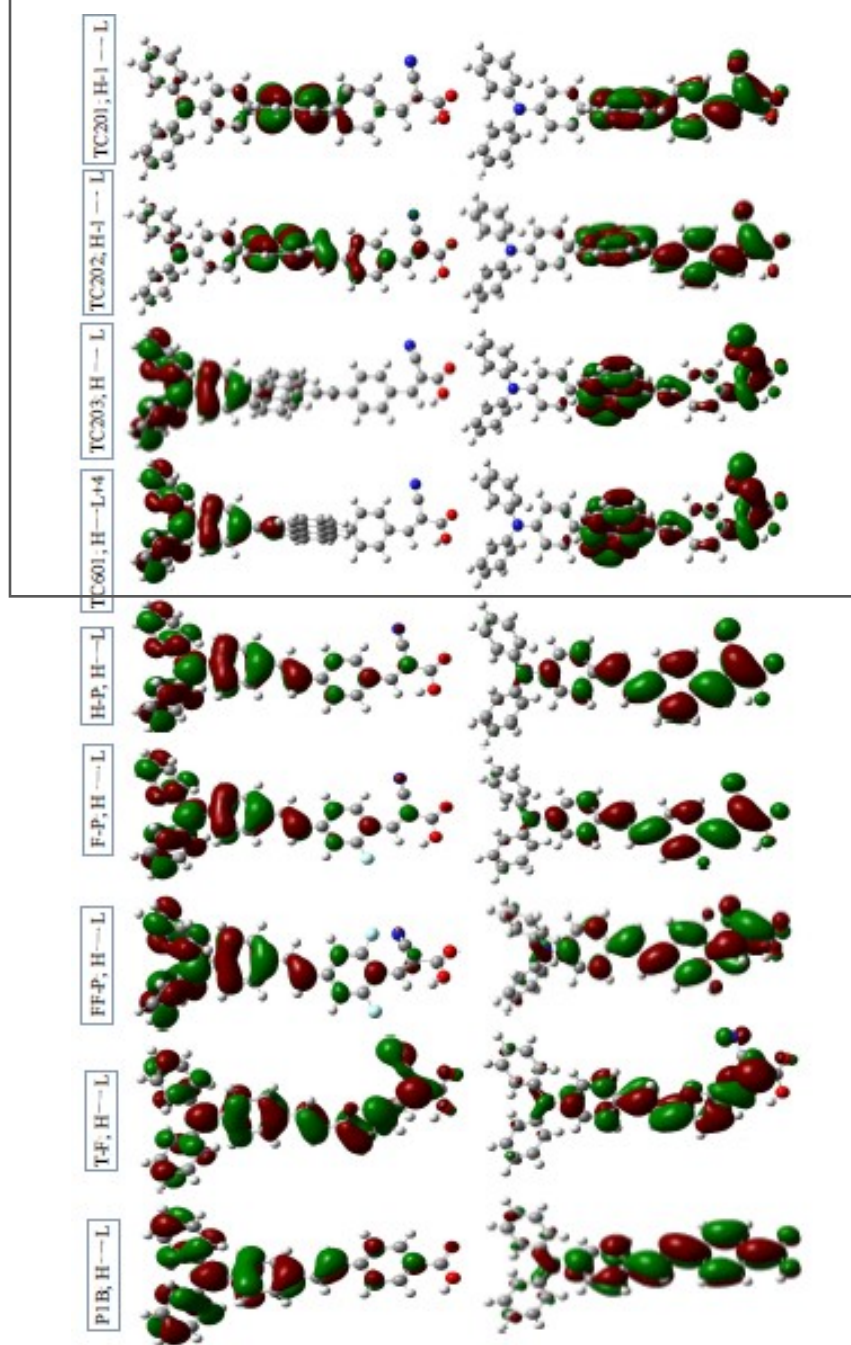
FIGURE 5 The distribution of the frontier molecular orbitals in triphenylamine-based dyes.

To understand the photovoltaic processes in the solar cells, more comprehensively, charge transfer characteristics, such as the excited-state lifetime of the dyes (τ), polarization (α), charge transfer distance (D_{CT}) and the overlap of the e-h distributions (S) were calculated and shown in Table 2.

TABLE 2 Excited-state lifetime of the dyes (τ), polarization (α), charge transfer distance (D_{CT}), and overlap of the e-h distributions (S).

Dye	$10^{-16}\tau$ (s)	α (a.u.)	D_{CT} (Å)	S
TC201	2.03	569.30	6.98	0.14
TC202	2.21	632.53	3.15	0.52
TC203	2.31	658.13	2.69	0.49
TC601	1.63	623.66	10.27	0.01
H-P	2.16	477.01	7.36	0.22
F-P	2.18	478.33	3.86	0.38
FF-P	2.11	462.23	3.17	0.40
T-F	2.35	437.80	7.63	0.14
P1B	1.92	393.12	3.69	0.36

According to Table 2, TC601 having the ethinyl anthracene phenyl as the π-conjugated system shows the highest charge transfer distance (D_{CT}) and the least electron-hole distribution overlap (S) than other dyes, in which the presence of a triple bond near the triphenylamine group increases the resonance effect of the π-

electrons that facilitates the charge transfer process. Moreover, TC203 represents the highest polarization against the incident light due to the lower energy band gap than other dyes. On the other hand, the relationship between the electronic chemical hardness and polarization and excited-state lifetime is shown in Figure 6. TC203 shows the lowest electronic chemical hardness, which facilitates the polarization of the molecule against the light. Considering Table 2 and Figure 6, it is confirmed that T-F, TC203, and TC202 have the highest excited-state lifetime, which can be attributed to the low chemical hardness of these dyes in comparison with other compounds.
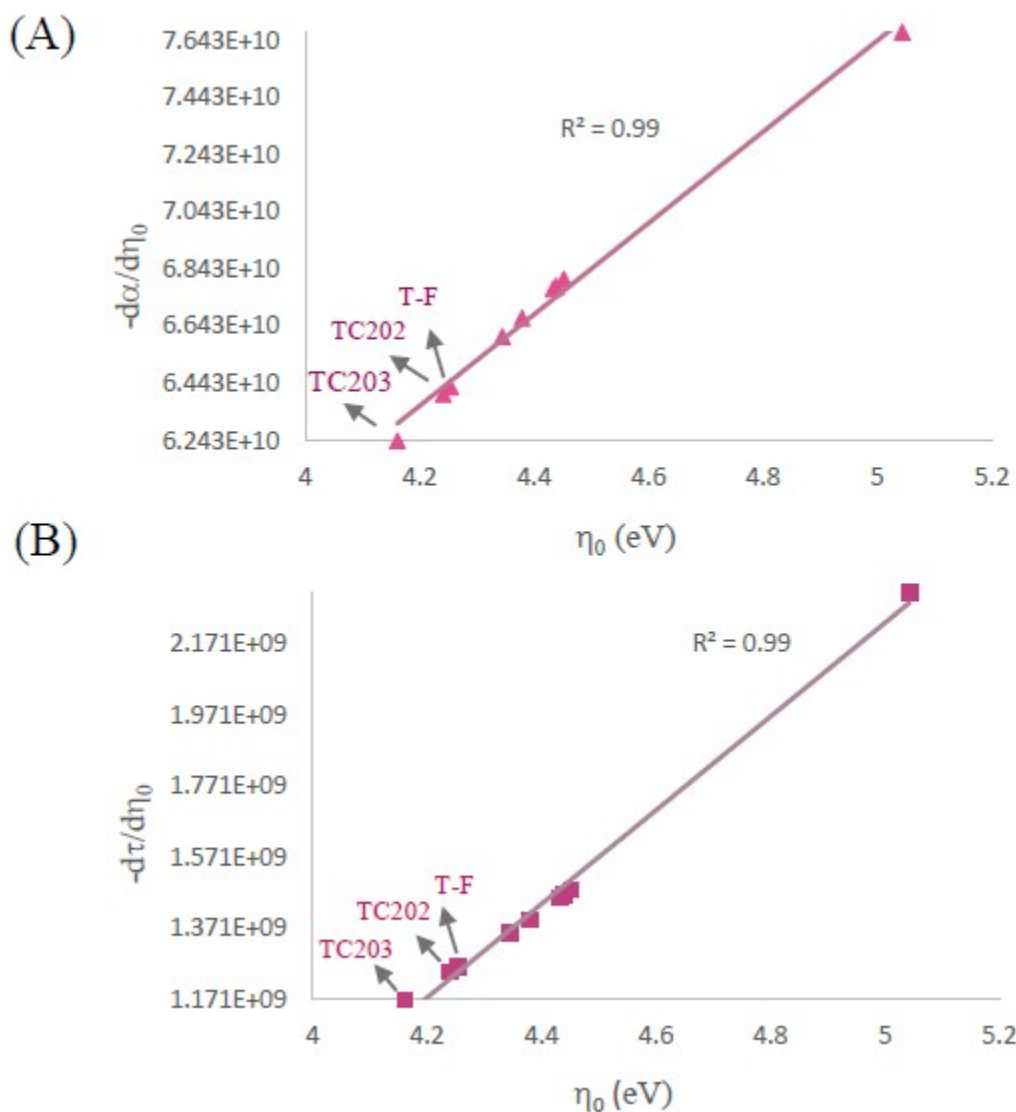
FIGURE 6 The relationship between the electronic chemical hardness and Polarization (A), and Excited-state lifetime (B).

3.2 | The kinetics and dynamics of charge transfer

Theoretical values of the exciton radius (a_x), exciton binding energy (EBE), the coupling constant of photosensitizers/TiO$_2$, (V_{RP}), charge transfer rate constant

between the dye and TiO$_2$, (k_{inj}), the rate of the exciton formation (R_a) and the rate of the exciton dissociation (R_d) are reported in Table 3.

TABLE 3 Exciton radius (a_x), exciton binding energy (EBE), the coupling constant of photosensitizers/TiO$_2$, (V_{RP}), charge Transfer rate constant between the dye and TiO$_2$, (k_{inj}), the rate of the exciton formation (R_a) and the rate of the exciton dissociation (R_d).

| Dye	a_x (Å)	EBE (eV)	V_{RP} (eV)	k_{inj} (s^{-1})	$10^{-8} R_a$ (s^{-1})	$10^{-49} R_d$ (s^{-1})
TC201	2.00	1.19	1.28	0.04	0.17	0.81
TC202	1.90	1.26	1.27	0.01	0.13	0.71
TC203	1.83	1.30	1.29	0.00	0.12	0.66
TC601	5.90	0.40	1.30	1.19	1.50	3.77
H-P	1.80	1.33	1.25	0.03	0.13	0.68
F-P	1.81	1.32	1.29	0.01	0.13	0.68
FF-P	1.78	1.34	1.29	0.01	0.14	0.69
T-F	1.65	1.44	1.21	0.02	0.10	0.57
P1B	1.47	1.62	1.21	0.84	0.14	0.59

According to Table 3, TC601 has the highest values of the exciton formation/dissociation rate and the lowest EBE value. Also, linear correlations between the rate of exciton formation and exciton binding energy, as well as the rate of the exciton dissociation with the exciton binding energy and exciton are depicted in Figure 7. Based on Figure 7A, a decrease in the EBE, increases the tendency of e-separation from the hole that results in fast exciton formation. Also, as shown in Figure 7B, the R_d values of the dyes are improved by the decrease in

the exciton binding energy, which facilitates the exciton separation and charge transfer. Moreover, in the cases of the dyes having a larger exciton radius, the less energy is required to separate the electron-hole pair. Based on the results, theoretically trend in the exciton radius is as follows:

P1B < T-F < FF-P < H-P < F-P < TC203 < TC202 < TC201 < TC601
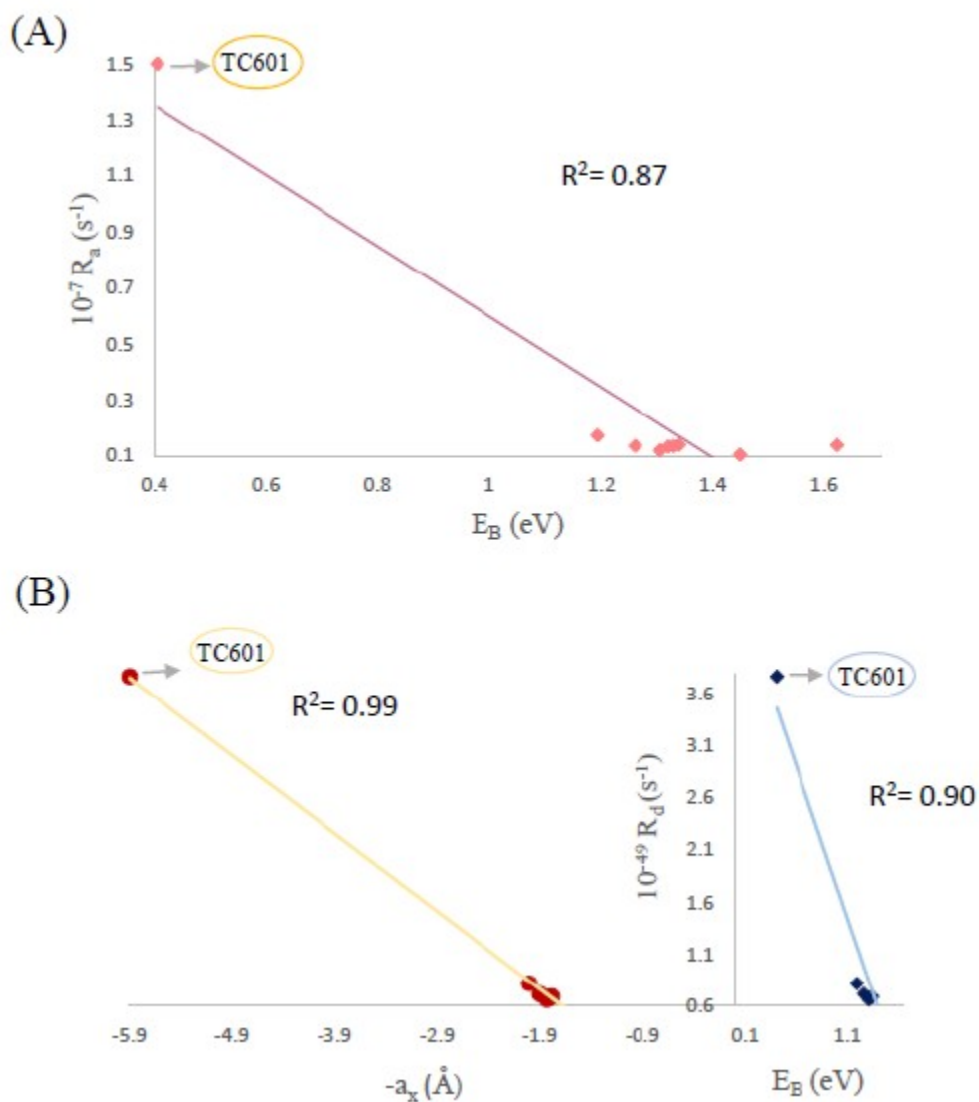
FIGURE 7 The linear correlation R_a/EBE (A), and R_d/EBE and R_d/a_x (B).

According to Figure 8A, IPCE changes as a function of ΔG_{inj}, which shows that the Gibbs energy of the electron injection from the excited states of the dye to the semiconductor directly affects the IPCE. Also, IPCE is highly dependent on the k_{inj} changes. TC601 has the highest values of the IPCE and k_{inj} due to the extended π-conjugated system. Because the presence of the π-conjugated system increases the resonance effect and also, light-harvesting ability and activity of the dye molecules against incident photons. On the other hand, Figure 8B shows the histograms of k_{inj} changes within ΔG_{inj}, in which the rate constant of the charge transfer decreases by a reduction in ΔG_{inj}. TC601 dye has the least energy barrier against the charge transfer to the TiO_2 semiconductor that facilitates photovoltaic processes on the TiO_2/dye interfaces.

(A)

(B)
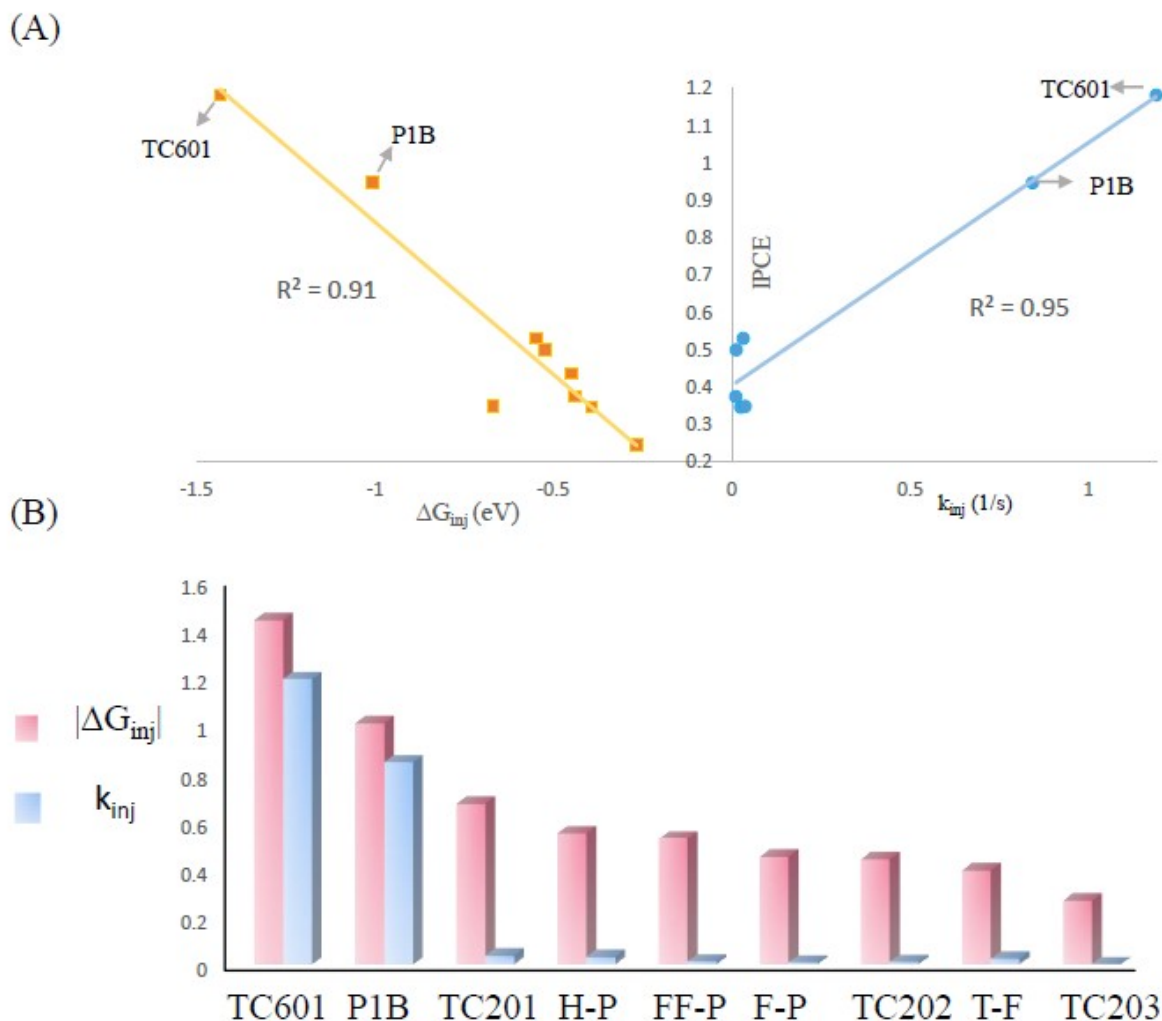
FIGURE 8 A, The linear correlation of IPCE with ΔG_{inj} and k_{inj}. B, The histograms of k_{inj} and ΔG_{inj} for the studied dyes.

The theoretical behavior of k_{inj} as a function of V_{RP} is shown by a polynomial function in Figure 9. According to the differential plot at the right side, an increase in V_{RP} values increase the dependence of the rate constant of the electron injection on the V_{RP}, showing a positive effect on k_{inj}.
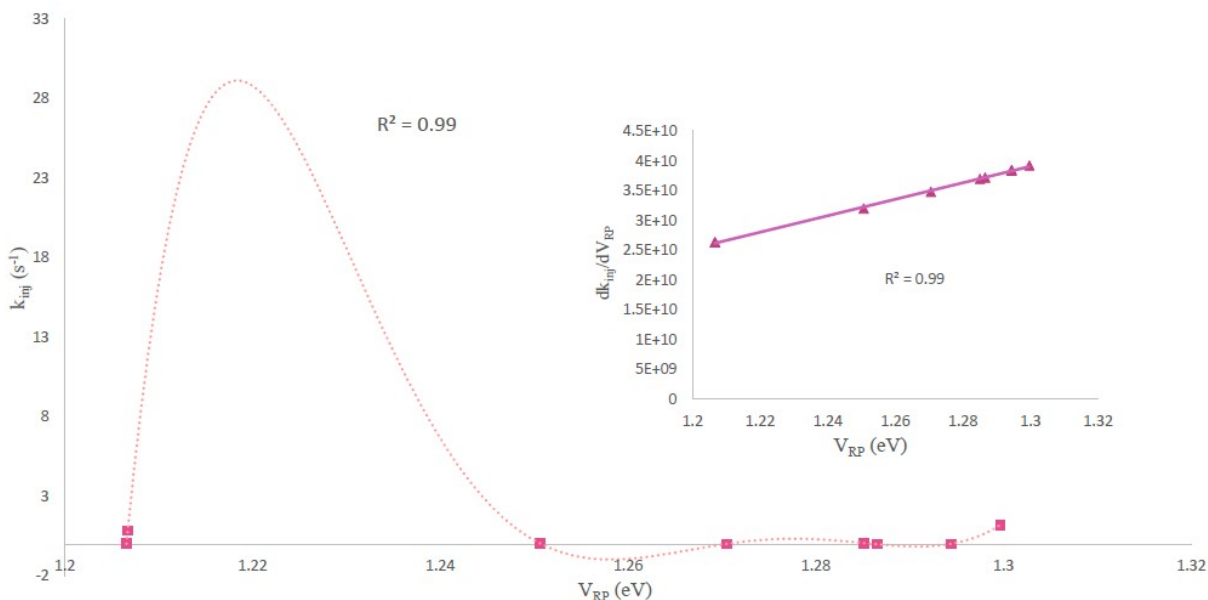
FIGURE 9 The theoretical correlation of k_{inj} and V_{RP} within their differential curve.

Theoretical behaviors of the IPCE and the rate of photon absorption/exciton dissociation are depicted in Figure 10. Based on this figure, TC601 having the ethinyl anthracene phenyl π-conjugated system shows the best photovoltaic properties from the kinetic point of view in terms of the exciton formation/dissociation rate compared to other dyes. The rate of exciton formation/dissociation into free charges in TC601 occurs faster than other dyes, which may be due to a higher electron transfer rate constant and also better coupling constant between the dye and TiO$_2$. The theoretically predicted trends in the exciton formation/dissociation rate, respectively, are as follow:

T-F < TC203 < F-P < H-P < TC202 < P1B < FF-P < TC201 < TC601

and

T-F < P1B < TC203 < H-P < F-P < FF-P < TC202 < TC201 < TC601

28
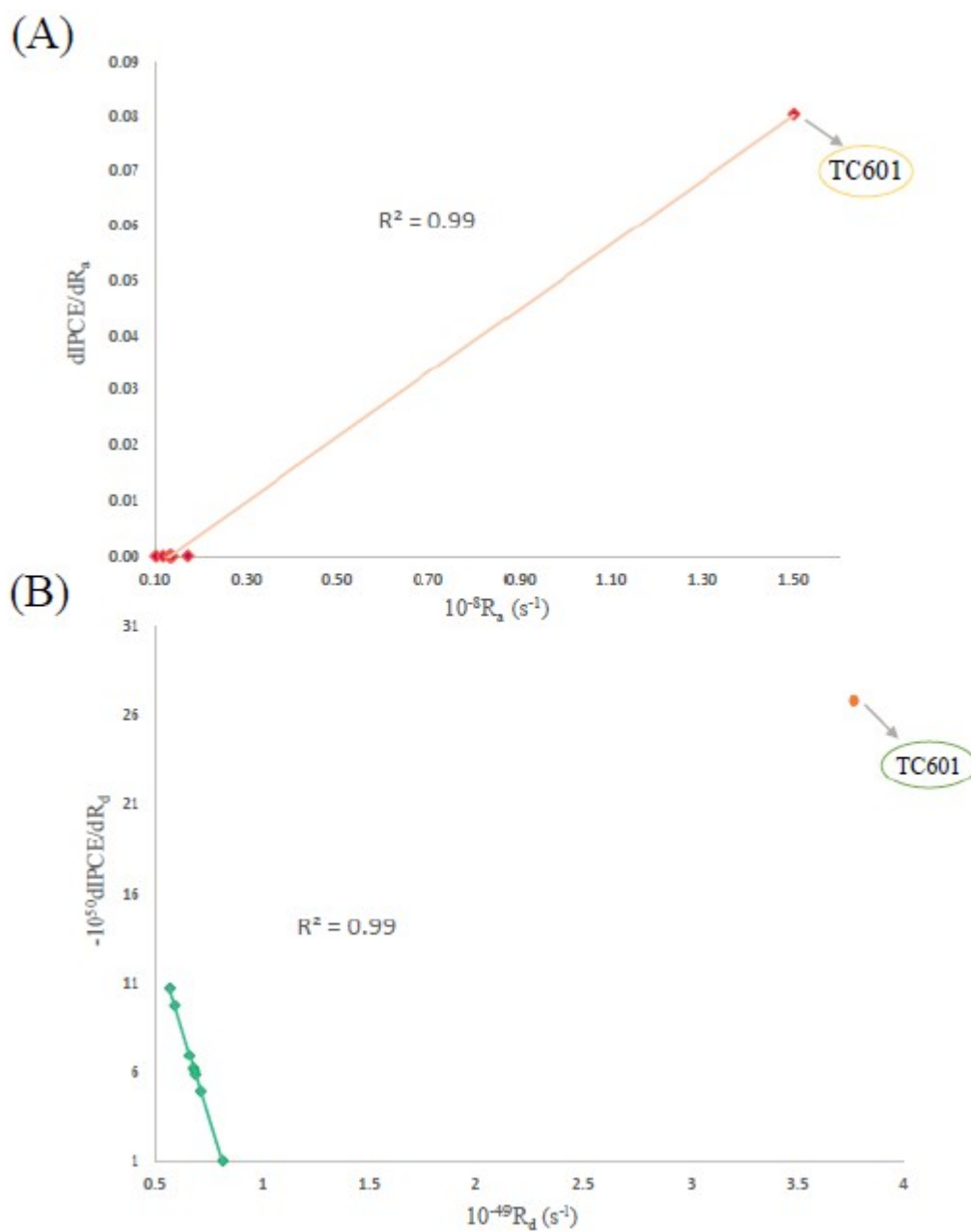
FIGURE 10 The possible correlation of the differential behavior of the IPCE with R_a (A), and R_d (B).

3.3 │ The simulation of the dye absorption spectrum within LHE and IPCE analyses

Based on TD-DFT calculations, the oscillator strengths (f), vertical excitation energy (E_{0-0}), maximum wavelength (λ_{max}), light-harvesting efficiency (LHE), incident photon to current conversion efficiency (IPCE) and main transitions of the dyes were calculated and represented in Table 4.

TABLE 4 Oscillator strength (f), vertical excitation energy (E0-0), maximum wavelength (λmax), main transition .s, light-harvesting efficiency (LHE), and incident photon to current conversion efficiency (IPCE)

Dye	f	E_{0-0} (eV)	λ_{max} (nm)	Major transition configuration and % transition		LHE	IPCE
TC201	0.32	3.24	382.63	H-1 ⟶ L	45.26	0.52	0.34
	0.15	3.47	356.81	H-1 ⟶ L+1	40.19	0.30	0.26
	0.00	3.80	326.26	H ⟶ L	40.19	0.01	0.01
	0.01	4.00	310.61	H-2 ⟶ L+1	40.19	0.01	0.02
	0.03	4.02	308.26	H ⟶ L	40.19	0.07	0.08
	0.01	4.06	305.22	H ⟶ L +4	40.20	0.03	0.04
TC202	0.84	2.98	415.93	H-1 ⟶ L	39.96	0.85	0.37
	0.00	3.53	351.41	H ⟶ L+1	44.12	0.01	0.01
	0.00	3.61	343.35	H ⟶ L	44.31	0.01	0.01
	0.00	3.96	313.25	H-3 ⟶ L+1	33.14	0.01	0.01
	0.76	4.04	306.71	H-2 ⟶ L	59.45	0.82	1.24
	0.04	4.06	305.68	H ⟶ L+4	40.06	0.09	0.13
TC203	1.16	2.85	434.32	H ⟶ L	43.98	0.93	0.24

TABLE 4 (continued)

Dye	f	E_{0-0} (eV)	λ_{max} (nm)	Major transition configuration and % transition		LHE	IPCE
	0.00	3.42	362.09	H-1 → L	44.07	0.01	0.01
	0.04	3.58	346.54	H-1 → L+1	41.90	0.08	0.08
	0.00	3.92	316.09	H-3 → L+1	28.84	0.01	0.01
	0.01	4.07	304.58	H → L+3	43.45	0.03	0.04
	0.27	4.11	301.51	H → L+1	29.96	0.44	0.68
TC601	0.53	3.20	387.73	H-1 → L	50.98	0.70	0.42
	0.07	3.42	362.88	H-1 → L+1	51.16	0.14	0.12
	0.00	3.65	339.84	H → L+1	58.07	0.00	0.01
	0.00	3.97	312.58	H → L	72.44	0.01	0.00
	0.76	4.03	307.32	H → L+4	91.03	0.82	1.18
	0.02	4.08	303.84	H → L+5	56.04	0.05	0.08
H-P	1.56	3.05	406.72	H → L	81.59	0.97	0.53
	0.02	4.01	308.96	H → L+2	32.93	0.05	0.08
	0.12	4.08	303.58	H-1 → L	55.66	0.24	0.39
	0.26	4.26	290.79	H → L+1	47.14	0.44	0.78
	0.18	4.34	285.82	H → L+5	54.35	0.34	0.62
	0.02	4.51	275.13	H-7 → L	54.76	0.05	0.10
F-P	1.54	3.02	410.06	H → L	81.74	0.97	0.43
	0.06	4.01	308.86	H → L+1	25.15	0.13	0.18
	0.12	4.06	304.94	H-1 → L	42.48	0.24	0.36

TABLE 4 (continued)

Dye	f	E_{0-0} (eV)	λ_{max} (nm)	Major transition configuration and %	LHE	IPCE

|				transition			
	0.18	4.35	284.64	H ⟶ L+5	57.91	0.33	0.59
	0.02	4.45	278.77	H-7 ⟶ L	46.23	0.04	0.08
FF-P	1.39	3.11	398.36	H ⟶ L	77.88	0.95	0.50
	0.03	4.01	309.15	H ⟶ L+2	39.57	0.05	0.08
	0.08	4.11	301.96	H-1 ⟶ L	38.44	0.16	0.24
	0.35	4.30	288.40	H-1 ⟶ L	33.19	0.55	0.94
	0.20	4.36	284.51	H ⟶ L+5	55.85	0.37	0.66
	0.01	4.48	276.87	H-4 ⟶ L	78.89	0.03	0.06
T-F	0.94	2.80	441.89	H ⟶ L	82.78	0.88	0.34
	0.18	3.81	325.06	H-1 ⟶ L	73.54	0.34	0.48
	0.09	4.00	309.62	H ⟶ L+1	37.02	0.18	0.29
	0.20	4.11	301.24	H ⟶ L+1	35.53	0.37	0.63
	0.19	4.34	285.78	H ⟶ L+6	74.54	0.35	0.67
	0.02	4.67	265.25	H ⟶ L+3	14.33	0.04	0.10
P1B	1.24	3.42	362.55	H ⟶ L	86.13	0.94	0.94
	0.04	4.02	308.01	H ⟶ L+1	55.87	0.08	0.13
	0.20	4.31	287.09	H ⟶ L+5	56.12	0.36	0.68
	0.15	4.49	276.00	H-1 ⟶ L	53.74	0.28	0.59
	0.05	4.70	264.34	H ⟶ L+9	19.34	0.11	0.25
	0.01	4.72	262.44	H ⟶ L+2	26.85	0.02	0.06
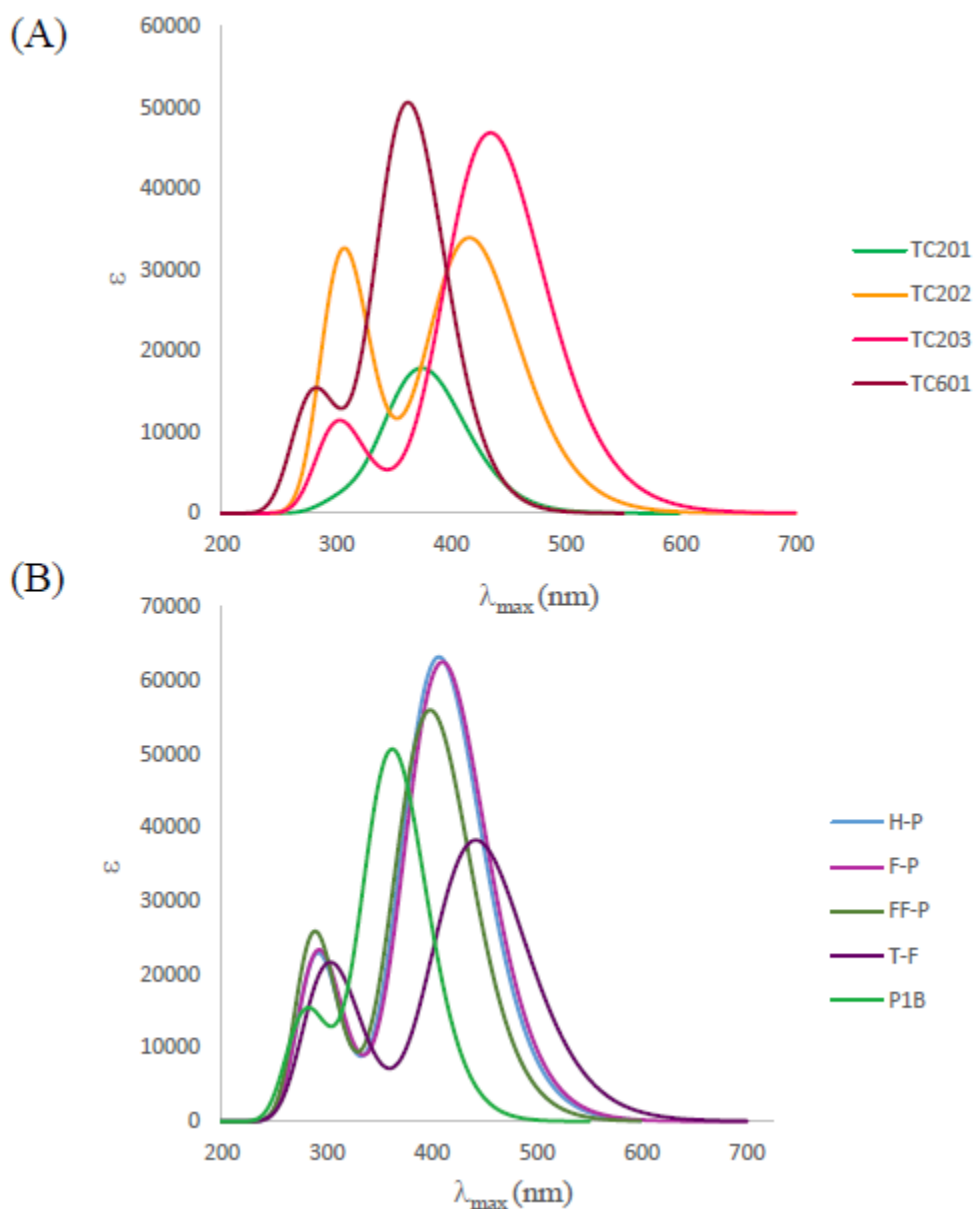
FIGURE 11 The simulated absorption spectra TC201, TC202, TC203 and TC601 dyes (A), H-P, F-P, FF-P, T-F and P1B (B).

According to the simulated absorption spectra in Figure 11 and data in Table 4, H-P and F-P have the highest molar absorption coefficient, which is due to the higher oscillator strength of electrons between their molecular orbitals that increases the probability of electron transfer from a lower level to a higher

electronic level. Also based on Figure 2, the energy levels of the molecular orbitals including H-3, H-2, H-1, H, L+3, L+2, L+1, and L indicate that for each compound H-3 and H-2 levels almost degenerated, while they are apart from the H-1 and H levels. Analogously, two contiguous energy levels of the L+3 and L+2 are also degenerated, while separated from L+1 and L level. Moreover, TC202, TC203, F-P, and T-F show a red-shift in comparison with other dyes, due to their smaller energy gap that decreases the energy of electron excitation, shifting the wavelength to higher values.

The results of the simulation of the IPCE and LHE behavior as the function of wavelength are shown in Fig. 12. Based on this figure, the IPCE values of the dyes do not follow the same in trend comparison with LHE. This means that the dyes having a high ability of light capture do not show a high ability to convert light into electricity, and vice versa. Also, the maximum values of IPCE and LHE are in the UV region, according to Figure 12.

The absorption spectrum behavior of these compounds does not match with the IPCE efficiency as a function of wavelength, but the trend of absorption spectra shift in these compounds is almost in agreement with the shift of LHE behavior of the dyes based on the absorption wavelengths. According to Figure 12B, H-P and F-P dyes have the highest LHE, which can be attributed to the high oscillator strength of these two compounds compared to other dye molecules.
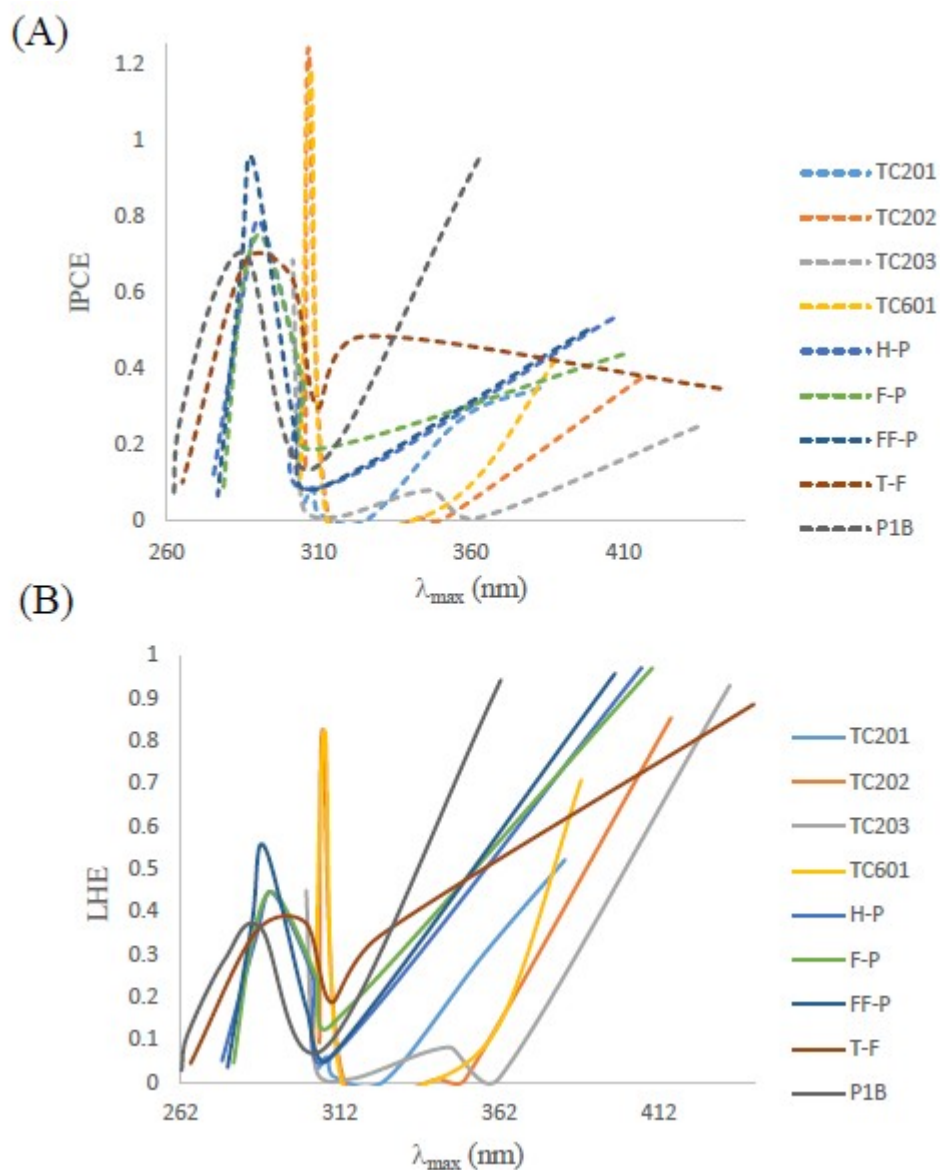
FIGURE 12 The theoretical behaviors of the light harvesting efficiency (LHE) (A), and Incident photon to current conversion efficiency (IPCE) as the functions of the maximum absorption wavelength (B).

The histograms of the electric dipole moment with the oscillator strengths are shown in Figure 13. The dyes having a high electric dipole moment represent a

higher oscillator strength that increases the possibility of electron transfer between the molecular orbitals, yielding a higher light-conversion efficiency.
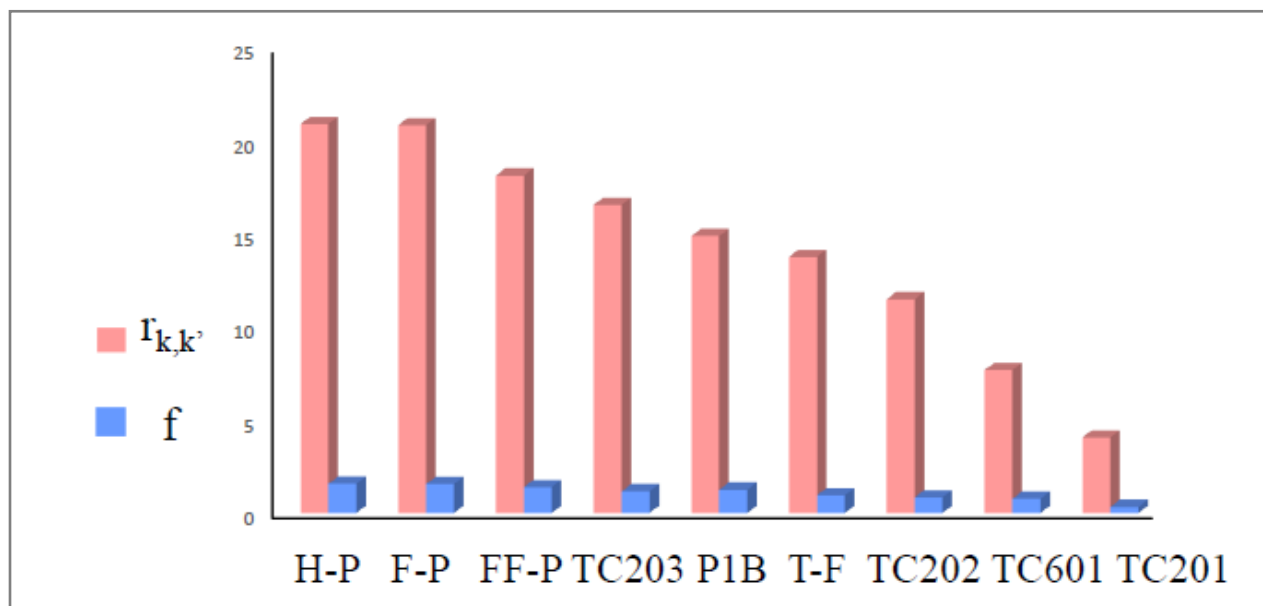
**FIGURE 13** The histograms of $r_{k,k'}$ and f for the studied dyes.

3.4 | The theoretical behavior of the voltage-current

The theoretical values of the photovoltaic parameters of the studied dyes, such as open-circuit voltage (V_{OC}), short circuit current density (J_{SC}), fill factor (FF) and solar cell efficiency (η_0) were calculated and reported in Table 5.

TABLE 5 Open circuit voltage (V_{OC}), short circuit current density (J_{SC}), fill factor (FF), and solar cell efficiency (η_0).

Dye	V_{OC} (V)	J_{SC} (mA/cm^2)	FF	η_0 (%)
TC201	3.99	10.78	0.96	0.41
TC202	3.81	12.59	0.95	0.46
TC203	3.71	8.66	0.95	0.31
TC601	4.02	29.31	0.96	1.13
H-P	3.95	17.43	0.96	0.66
F-P	3.91	14.45	0.96	0.54
FF-P	4.02	16.10	0.96	0.62
T-F	3.82	12.39	0.95	0.45
P1B	4.63	27.72	0.96	1.24

According to Table 5, P1B having the benzoic acid as the electron acceptor in comparison with the dyes having cyanoacrylic acid as the electron acceptor shows the highest values of open-circuit voltage, fill factor and efficiency. These properties show the greater ability of the electron-withdrawing by benzoic acid compared to the cyanoacrylic acid. On the other hand, TC601 shows the highest amount of short circuit current density due to the higher π-resonance effect. Based on the data in Table 5, the voltage-current curve of the studied dyes is shown in Figure 14. According to this figure, the highest values of the open-circuit voltage and short circuit current density are related to P1B and TC601 dyes, respectively.
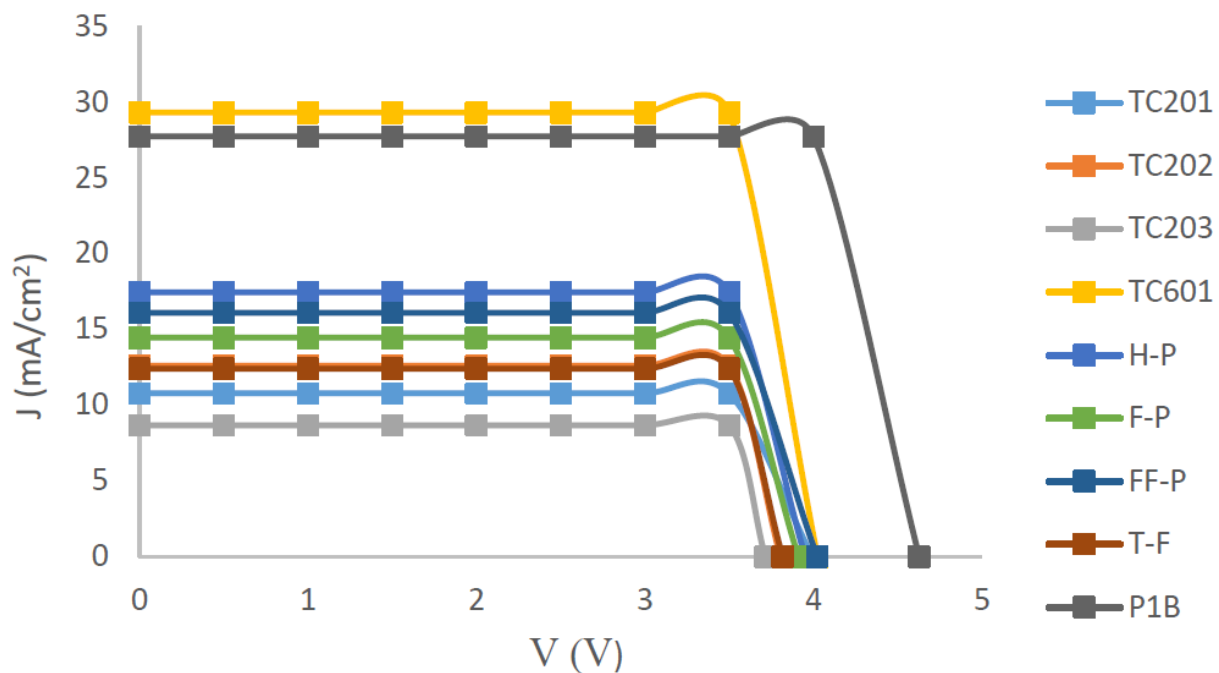
FIGURE 14 The simulated curve of the voltage-current dyes based on triphenylamine.

Also, the linear correlations of V_{OC} and FF as a function of the quantum reactivity indices including electronic chemical potential (μ) and global electrophilicity (ω) are depicted in Figure 15. By reducing the electrophilicity, the tendency of electron absorption decreases that improves the values of the open-circuit voltage and fill factor. Also, a decrease in the absolute value of the electronic chemical potential, the open-circuit voltage and fill factor are improved. Among all the studied dyes, P1B having the benzoic acid as the electron acceptor shows the most favorable photovoltaic properties in terms of open-circuit voltage and fill factor.
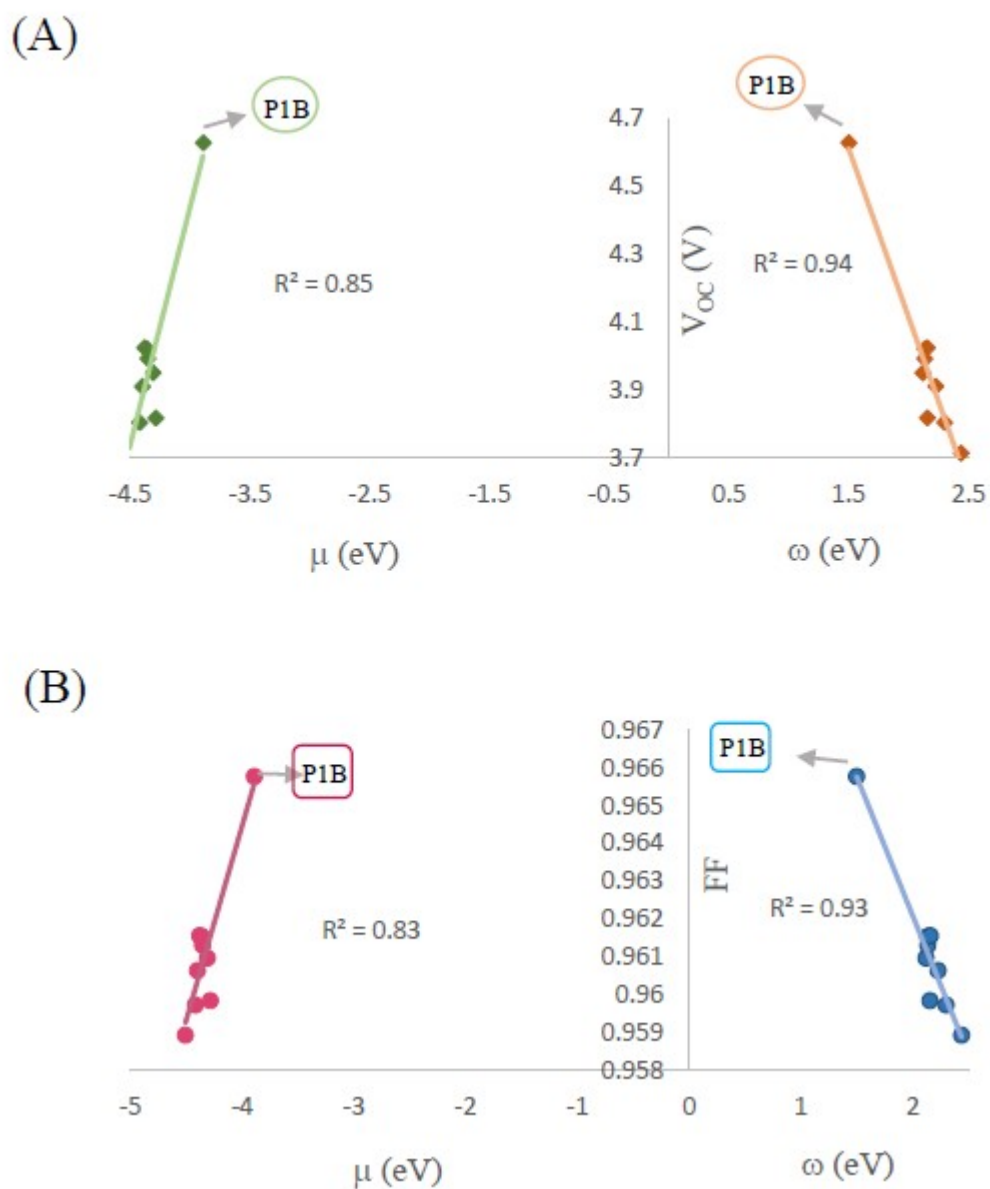
FIGURE 15 Linear relationship of V_{OC} with μ and ω (A), FF with μ and ω (B).

Also, the relationship between the final efficiency of the solar cells and the short circuit current density with IPCE is shown in Figure 16. Based on this figure, the dyes having a high ability of IPCE show greater efficiency and higher values of short circuit current density.
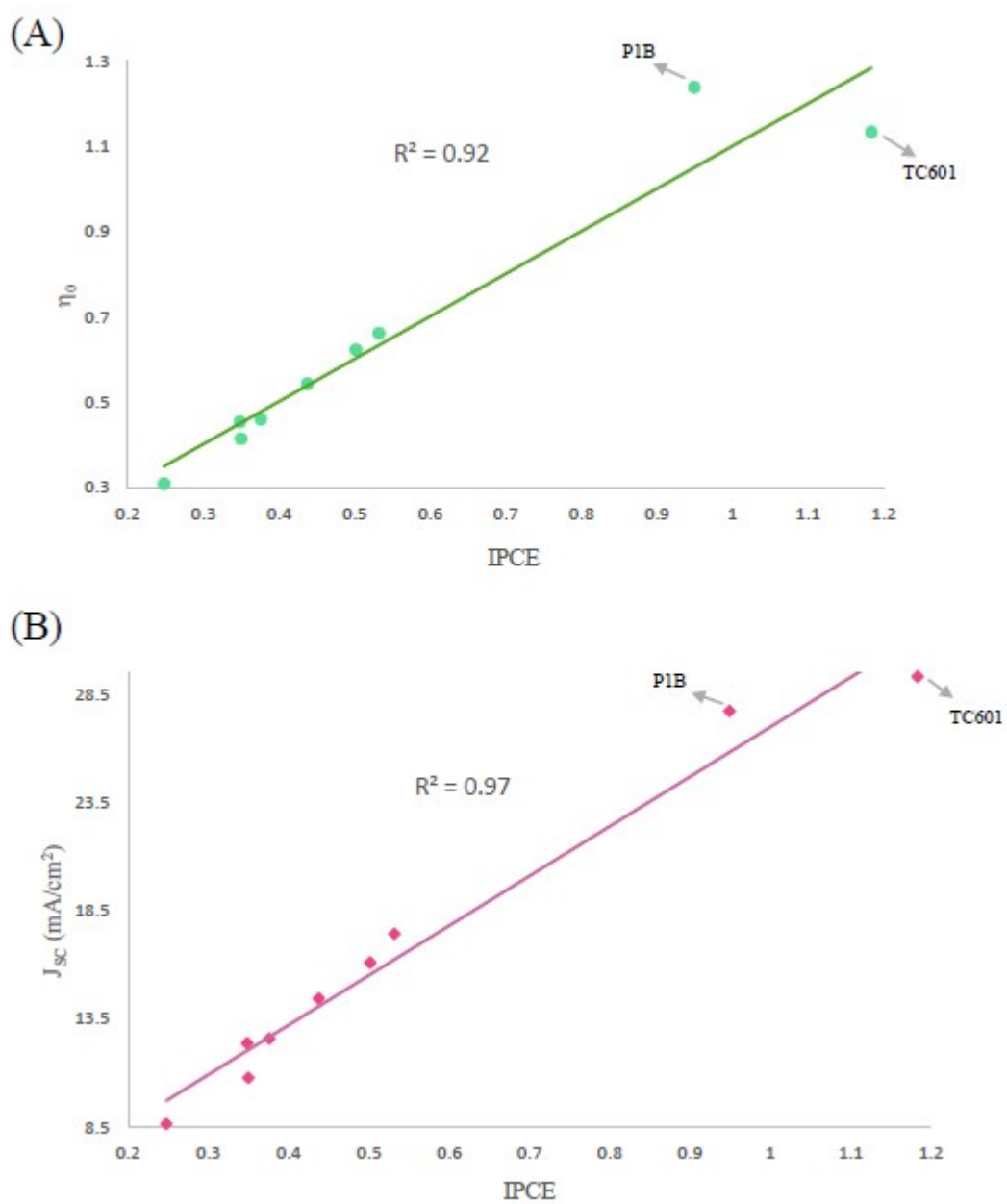
FIGURE 16 Linear correlation of the IPCE with the final efficiency (A), Short-circuit current density (B).

4 | Conclusions

In this research, a theoretical study was performed on a series of metal-free organic dyes containing a triphenylamine moiety as the electron donor, cyanoacrylic acid and benzoic acid moiety as the electron acceptors and different π-conjugated systems. These dyes were analyzed to evaluate their feasibility of using as the sensitizers in the DSSCs. On the basis of the obtained results, a linear correlation between the incident photon to current conversion efficiency (IPCE) and $k_{inj}/\Delta G_{inj}$ of the dyes has been obtained. Also, some correlations between the quantum reactivity indices and photovoltaic parameters were obtained and discussed. Based on the charge transfer indices at the dye/TiO₂ interface, TC601 dye represents the larger charge transfer distance and small overlap of the electron-hole distribution than other dyes. Also, this dye has the highest values of photon absorption rate (R_a), exciton dissociation rate (R_d), and the lowest value of the exciton binding energy (EBE). Moreover, the absorption spectrum of the dyes and the behaviors of the IPCE and LHE as the functions of the wavelength was examined, showing that H-P and F-P dyes have the higher molar absorption coefficients and LHE in comparison with other dyes. Also, TC202, TC203, F-P, and T-F dyes show a red-shift. Finally, TC601 is the best candidate among the nine studied compounds due to lower electron transfer Gibbs energy, better kinetic

behavior and charge transfer properties, higher short-circuit current density and energy conversion efficiency.

ACKNOWLEDGMENT

REFERENCES

[1] A. Singh, P. Baredar, B. Gupta, *Energy Convers. Manage*. **2017**, 145, 398.

[2] E. Kabir, P. Kumar, S. Kumar, A. A. Adelodun, K. H. Kim, *Renew. Sust. Energy. Rew*. **2018**, 82, 894.

[3] A. Błaszczyk, *Dyes Pigm*. **2018**, 149, 707.

[4] P. P. Kumavat, P. Sonar, D. S. Dalal, *Renew. Sust. Energy. Rew*. **2017**, 78, 1262.

[5] K. Moustakas, M. Loizidou, M. Rehan, A. S. Nizami, *Renew. Sust. Energy. Rew*. **2020**, 119, 109418.

[6] D. U. Lawal, N. A. Qasem, *Renew. Sust. Energy. Rew*. **2020**, 125, 109817.

[7] H. A. Maddah, V. Berry, S. K. Behura, *Renew. Sust. Energy. Rew*. **2020**, 121, 109678.

[8] J. G. Krishna, P. K. Ojha, S. Kar, S. K. Roy, J. Leszczynski, *Nano Energy* **2020**, 70, 104537.

[9] M. Talaat, M. A. Farahat, M. H. Elkholy, *Energy* **2019**, 170, 668.

[10] S. Sharma, B. Siwach, S. K. Ghoshalc, D. Mohan, *Renew. Sust. Energy. Rew*. **2017**, 70, 529.

[11] X. Xie, Z. Liu, F. Q. Bai, H. X. Zhang, *Comput. Theor. Chem*. **2019**, 1154, 44.

[12] X. Song, X. Yang, H. Wang, J. An, Z. Yu, X. Wang, A. Hagfeldt, L. Sun, *Sol Energy* **2019**, 187, 274.

[13] B. O'Regan, M. Gr€atzel, *Nature* **1991**, 353, 737.

[14] C. Dong, W. Xiang, F. Huang, D. Fu, W. Huang, U. Bach, Y. B. Cheng, X. Li, L. Spiccia, *Nanoscale* **2014**, 6, 3704.

[15] N. V. Krishna, J. V. Krishna, M. Mrinalini, S. Prasanthkumar, L. Giribabu, *ChemSusChem* **2017,** 23, 4668.

[16] B. Xu, Y. Li, P. Song, F. Ma, M. Sun, *Sci. Rep.* **2017**, 7, 45688.

[17] M. H. Yeh, Y. A. Leu, W. H. Chiang, Y. S. Li, G. L. Chen, T. J. Li, L. Y. Chang, L. Y. Lin, J. J. Lin, K. C. Ho, *J. Power Sources* **2018**, 375, 29.

[18] F. G. Nesheli, M. Tajbakhsh, B. Hosseinzadeh, R. Hosseinzadeh, *J. Photochem. Photobiol. A* **2020**, 112521.

[19] X. Xie, Z. Liu, W. Li, F. Q. Bai, E. C. Lee, H. X. Zhang, *Chem. Phys. Lett.* **2019**, 719, 39.

[20] J. Wang, K. Liu, X. Zhan, Chem. Rew. **2016**, 116, 14675.

[21] G. Richhariya, A. Kumar, P. Tekasakul, B. Gupta, *Renew. Sust. Energy. Rew.* **2017**, 69, 705.

[22] L. Zhang, J. M. Cole, *ACS Appl. Mater. Interfaces* **2015**, 7, 3427.

[23] Y. Fu, B. Li, L. Haizhen, B. Xue, E. Liu, *Mater. Chem. Phys.* **2020**, 239, 121970.

[24] W. Li, W. Ren, Z. Chen, T. F. Lu, L. Deng, J. Tang, X. Zhang, L. Wang, F. Q. Bai, *Sol Energy* **2019**, 188, 742.

[25] Y. Qin, Q. Peng, *Int. J. Photoenergy* **2012**, 2012, 21.

[26] M. K. Nazeeruddin, A. Kay, I. Rodicio, R. Humphry-Baker, E. Müller, P. Liska, N. Vlachopoulos, M. Grätzel, *J. Am. Chem. Soc.* **1993**, 115, 6382.

[27] Y. Chi, C. H. O. U. Chun-Cheng, K. L. Wu, *Google Patents* **2012**, 8, 507.

[28] A. Dhar, N. S. Kumar, P. K. Paul, S. Roy, R. L. Vekariyae, *Org. Electron.* **2018**, 53, 280.

[29] G. Deogratias, N. Seriani, T. Pogrebnaya, A. Pogrebnoi, *J. Mol. Graph* **2020**, 94, 107480.

[30] S. Jiang, S, Y. Chen, Y. Li, L. Han, *J. Photochem. Photobiol. A* **2019**, 384, 112031.

[31] J. Zhang, C. J. Chen, H. C. Zhu, *Appl. Surf. Sci.* **2020**, 513, 145844.

[32] V. Mohankumar, P. Pounraj, M. S. Pandian, P. Ramasamy, *J. Mol. Struct.* **2019**, 1195, 494.

[33] H. Wu, Z. Huang, T. Hua, C. Liao, H. Meier, H. Tang, L. Wang, D. Cao, *Dyes Pigm.* **2019**, 165, 103.

[34] A. Dhar, N. S. Kumar, A. A. Ibrahim, R. L. Vekariya, *Org. Electron.* **2018**, 56, 232.

[35] H. Zhang, Z. E. Chen, J. Hu, Y. Hong, *Dyes Pigm.* **2019**, 164, 213.

[36] M. R. Elmorsy, R. Su, A. A. Fadda, H. A. Etman, E. H. Tawfik, A. El-Shafei, *Dyes Pigm* **2018**, 158, 121.

[37] T. F. Lu, W. Li, H. X. Zhang, *Org. Electron.* **2018**, 59, 131.

[38] R. Yuan, L. Zhang, L. Chen, H. Zhang, P. Dou, X. Ren, W. Chen, H. Zhou, Y. Wan, H. Wu, *Tetrahedron Lett.* **2019**, 60, 1803.

[39] Y. Li, J. Liu, D. Liu, X. Li, Y. Xu, *Comput. Mater. Sci.* **2019**, 161, 163.

[40] M. R. Elmorsy, R. Su, A. A. Fadda, H. A. Etman, E. H. Tawfik, A. El-Shafei, *New J. Chem.* **2018**, 42, 11430.

[41] D. P. Hagberg, T. Marinado, K. M. Karlsson, K. Nanomura, P. Qin, G. Boschloo, T. Brinck, A. Hagfeldt, L. Sun, *J. Org. Chem.* **2007**, 72, 9550.

[42] M. Hosseinnezhad, S. Moradian, K. Gharanjig, *Dyes Pigm.* **2015**, 123, 147.

[43] F. Li, Y. Z. Zhu, S. C. Zhang, H. Gao, B. Pan, J. Y. Zheng, *Dyes Pigm.* **2017**, 139, 292.

[44] M. U. Khan, M. Ibrahim, M. Khalid, S. Jamil, A. A. Al-Saadi, M. R. S. A. Janjua, *Chem. Phys. Lett.* **2019**, 719, 59.

[45] P. Naik, R. Su, M. R. Elmorsy, D. D. Babu, A. El-Shafei, A. V. Adhikari, *J. Photochem. Photobiol. A* **2017**, 345, 63.

[46] A. Mahmood, *Sol Energy* **2016**, 123, 127.

[47] P. Pounraj, V. Mohankumar, M. S. Pandian, P. Ramasamy, *J. Mol. Graph.* **2018**, 79, 235.

[48] S. H. Kim, J. Choi, C. Sakong, J. W. Namgoong, W. Lee, D. H. Kim, B. Kim, M. J. Ko, J. P. Kim, *Dyes Pigm.* **2015**, 113, 390.

[49] Z. Yang, C. Liu, C. Shao, C. Lin, Y. Liu, *J. Phys. Chem. C* **2015**, 119, 21852.

[50] M. Bourass, A. T. Benjelloun, M. Benzakour, M. Mcharfi, F. Jhilal, M. Hamidi, M. Bouachrine, *New J. Chem.* **2017**, 41, 13336.

[51] R. Dutta, S. Kalita, D. J. Kalita, *Comput. Theor. Chem.* **2018**, 1142, 39.

[52] N. Wazzan, A. Irfan, *Org. Electron.* **2018**, 63, 328.

[53] A. Irfan, *Comput. Theor. Chem.* **2019**, 1159, 1.

[54] C. Teng, X. Yang, C. Yang, S. Li, M. Cheng, A. Hagfeldt, L. Sun, *J. Phys. Chem. C* **2010**, 114, 9101.

[55] J. T. Lin, P. C. Chen, Y. S. Yen, Y. C. Hsu, H. H. Chou, P. M. C. Yeh, *Org. Lett.* **2009**, 11, 97.

[56] Y. D. Lin, T. J. Chow, *J. Photochem. Photobiol. A* **2012**, 230, 47.

[57] Y. D. Lin, C. T. Chien, S. Y. Lin, H. H. Chang, C. Y. Liu, T. J. Chow, *J. Photochem. Photobiol. A* **2011**, 222, 192.

[58] A. A. Youssef, S. M. Bouzzine, Z. M. E. Fahim, I. Sıdır, M. Hamidi, M. Bouachrine, *Physica B Condens. Matter* **2019**, 560, 111.

[59] M. E. Casida, C. Jamorski, K. C. Casida, D. R. Salahub, *J. Chem. Phys. Chem.* **1998**, 108, 4439.

[60] E. D. Glendening, C. R. Landis, F. Weinhold, *Comput. Mater. Sci*. **2012**, 2, 1.

[61] T. Lu, F. Chen, *J. Comput. Chem*. **2012**, 33**,** 580.

[62] M. J. Frisch, G. W. Trucks, H. B. Schlegel, G. E. Scuseria, M. A. Robb, J. R. Cheeseman, J. A. Montgomery, Jr., T. Vreven, K. N. Kudin, J. C. Burant, J. M. Millam, S. S. Iyengar, J. Tomasi, V. Barone, B. Mennucci, M. Cossi, G. Scalmani, N. Rega, G. A. Petersson, H. Nakatsuji, M. Hada, M. Ehara, K. Toyota, R. Fukuda, J. Hasegawa, M. Ishida, T. Nakajima, Y. Honda, O. Kitao, H. Nakai, M. Klene, X. Li, J. E. Knox, H. P. Hratchian, J. B. Cross, V. Bakken, C. Adamo, J. Jaramillo, R. Gomperts, R. E. Stratmann, O. Yazyev, A. J. Austin, R. Cammi, C. Pomelli, J. W. Ochterski, P. Y. Ayala, K. Morokuma, G. A. Voth, P. Salvador, J. J. Dannenberg, V. G. Zakrzewski, S. Dapprich, A. D. Daniels, M. C. Strain, O. Farkas, D. K. Malick, A. D. Rabuck, K. Raghavachari, J. B. Foresman, J. V. Ortiz, Q. Cui, A. G. Baboul, S. Clifford, J. Cioslowski, B. B. Stefanov, G. Liu, A. Liashenko, P. Piskorz, I. Komaromi, R. L. Martin, D. J. Fox, T. Keith, M. A. Al-Laham, C. Y. Peng, A. Nanayakkara, M. Challacombe, P. M. W. Gill, B. Johnson, W. Chen, M. W. Wong, C. Gonzalez, J. A. Pople, GAUSSIAN 03, Revision C02 (Gaussian, Inc., Wallingford, CT, 2003).

[63] P. Ren, Y. Zhang, Z. Luo, P. Song, Y. Li, *J. Mol. Liq*. **2017**, 247, 193.

[64] M. L. Hossain, W. Qarony, S. Ma, L. Zeng, D. Knipp, Y. H. Tsang, *Nanomicro Lett* **2019**, 11, 58.

[65] N. M. Ravindra, B. Prasad, *Sol. Cells* **1980**, 2, 109.

[66] M. Prakasam, P. M. Anbarasan, *Mater. Today* **2019**, 9, 156.

[67] S. Sabagh, M. Izadyar, F. Arkan, *Int. J. Quantum Chem*. **2020**, 120, 26171.

[68] Y. Sheng, M. Li, M. M. Flores-Leonar, W. Lu, J. Yang, Y. Hu, *J. Mol. Struct*. **2020**, 1205, 127567.

[69] V. Sharma, P. K. Jha, *Sol. Energy Mater Sol. Cells* **2019**, 200, 109908.

[70] Y. Fu, T. Lu, Y. Xu, M. Li, Z. Wei, H. Liu, W. Lu, *Dyes Pigm*. **2018**, 155, 292.

[71] Y. Xu, X. Xu, M. Li, W. Lu, *Sol Energy* **2020**, 195, 82.

[72] F. Arkan, M. Izadyar, *Comput. Mater. Sci*. **2018**, 152, 324.

[73] F.Arkan, M. Izadyar, *Sol. Energy Mater Sol. Cells* **2018**, 180, 46.

[74] F.Arkan, M. Izadyar, *Appl. Phys. Lett*. **2019**, 115, 183903.

[75] F.Arkan, M. Izadyar, *Sol Energy* **2017**, 146, 368.

[76] F.Arkan, M. Izadyar, *Renew. Sust. Energy. Rew*. **2018**, 94, 609.

[77] F.Arkan, M. Izadyar, *Sol Energy* **2019**, 194, 51.

[78] F.Arkan, M. Izadyar, *Optik* **2020**, 203, 163972.

[79] F. Arkan, M. Izadyar, A. Nakhaeipour, *Renew. Sust. Energy. Rew*. **2017**, 9, 023502.

[80] S. B. Novir, S. M. Hashemianzadeh, *Curr. Appl. Physi*. **2014**, 14, 1401.

[81] Y. Xu, M. A. Schoonen, *Am. Mineral*. **2000**, 85, 543.

[82] H. Wu,T, Ma, C. Wu, L. Yan, Z. Su, *Dyes Pigm*. **2017**, 142, 379.

[83] T. Le Bahers, C. Adamo, I. Ciofini, *J. Chem. Theory Comput*. **2011**, 7, 2498.

[84] X. Xie, Z. Liu, F. Q. Bai, H. X. Zhang, *Comput. Theor. Chem*. **2019**, 1154, 44.

SUPPORTING INFORMATION

Additional supporting information may be found online in the Supporting Information section at the end of this article.